Fluids migration and dynamics of a blocks-and-faults system

A.M.Gabrielov[1,2], V.I.Keilis-Borok[3,4], V.Pinsky[5], O.M.Podvigina[4,6], A.Shapira[5,7], V.A.Zheligovsky[4,6]

[1]Department of Earth and Atmospheric Sciences,
Purdue University, W.Lafayette, IN 47907-1397, USA

[2]Department of Mathematics,
Purdue University, W.Lafayette, IN 47907-1395, USA

[3]Department of Earth and Space Sciences,
University of California, Los Angeles, CA 90095-1567, USA

[4]International Institute of Earthquake Prediction Theory
and Mathematical Geophysics,
Russian Academy of Sciences,
79 bldg.2, Warshavskoe ave., 117556 Moscow, Russian Federation

[5]Geophysical Institute of Israel,
P.O.B. 182, Lod 71100, Israel

[6]Laboratory of general aerodynamics,
Institute of Mechanics, Lomonosov Moscow State University
1, Michurinsky ave., 119899 Moscow, Russian Federation

[7]International Seismological Centre,
Pipers Lane, Thatcham, Berkshire, United Kingdom RG19 4NS

Abstract. A two-dimensional mathematical model of block structures of the Earth crust, which takes into account the influence of fluids migrating along tectonic faults, is presented in the paper. Results of numeric simulations based on the model for a regular "brick wall" structure. Collective motion of blocks is determined by geometry of the tectonic structure and by motion of confining blocks, and does not depend on the fluid regime. Spatial clustering of epicenters is observed. Patterns of the simulated earthquake flows depend on the boundary conditions for fluid. A reasonable qualitative agreement of the simulated earthquakes catalog and the catalog of the Geophysical Institute of Israel is found in simulations for the Israeli seismic region.

Keywords: earthquake catalog, block model, fault, tectonic structure, fluid, filtration

1 Introduction

Development and analysis of deterministic block models of the seismotectonic process became a rapidly expanding area of research after Burridge and Knopoff (1967) considered a one-dimensional slider-block model of a fault, and chaotic behaviour was observed in its numerous one- and two-dimensional modifications by Bak *et al.* (1987, 1988), Bak & Tang (1989), Carlson & Langer (1989a,b), Carlson *et al.* (1991), Carlson (1991). Similar models have been studied by Otsuka (1972), Ida (1978), Nur (1978), Cao & Aki (1985, 1986), Feder & Feder (1991), Rundle & Brown (1991), Christensen & Olami (1992), Olami & Christensen (1992), Huang *et al.* (1992), Narkounskaya *et al.* (1992), Myers & Langer (1993), Rice (1993), Shaw (1993), Ben-Zion & Rice (1993, 1995), Ghertzik (1993, 1994, 1998), Gabrielov *et al.* (1994), Hertz & Hopfield (1995), Schmittbuhl *et al.* (1996). In the next generation models of Bak *et al.* (1987, 1988), Bak & Tang (1989), Sornette & Sornette (1989), Ito & Matsuzaki (1990), Ito (1992), Nakanishi (1990, 1991), Brown *et al.* (1991), Chen *et al.* (1991), Lomnitz-Adler *et al.* (1992), Olami *et al.* (1992), Vasconcelos *et al.* (1992), Akishin *et al.* (1998) (the lists do not pretend to be complete) dynamics of block structures is represented by cellular automata.

The models exhibit chaotic behaviour and reproduce major empirical laws characterising observed seismicity. While this kind of modelling is an important tool for understanding of the processes in the Earth crust resulting in seismicity, the models have some natural limitations. The original uniform Burridge & Knopoff (1967) model is an idealisation of a single fault; it fails to reproduce aftershocks. To certain extent this deficiency is inherited by many subsequent models: commonly smooth isolated faults are considered, no account of the block system geometry being taken. This limitation is essential, because the geometry poses constraints on the possible motion of blocks, geometric incompatibility (see Gabrielov *et al.* 1996) being a manifestation of those. An open question remains, whether the complexity of seismicity, the richness of seismic phenomena, and the fundamental regularities such as the Gutenberg-Richter law are linked to fault segmentation and other heterogeneities, or instabilities of the underlying inertial dynamics dominate the behaviour (see discussion in Rice, 1993; Cochard & Madariaga, 1994, 1996; Madariaga & Cochard,

1994, 1996; Nielsen *et al.* 1995; Ben-Zion & Rice, 1995, 1997; Knopoff, 1996; Langer *et al.* 1996; Rice & Ben-Zion, 1996; Robinson & Benites, 1995; Ben-Zion *et al.* 1999; Lyakhovsky *et al.* 2001). The complexities in slip histories on a smooth fault can be sensitive to the details of constitutive equations and physical mechanisms incorporated into the model (see Ben-Zion & Rice, 1997); the question is complicated by the role of inadequate resolution in numeric simulations (see Rice, 1993; Ben-Zion & Rice 1993, 1995, 1997; Rice & Ben-Zion, 1996).

A family of two- and three-dimensional models of block structure of lithosphere have been developed at the International Institute of Earthquake Prediction Theory and Mathematical Geophysics (IIEPT), Moscow (see Gabrielov *et al.* 1986, 1990, 1993; Rozenberg & Soloviev, 1997), enabling one to take into account the actual shape of blocks constituting a tectonic region. (Note that while in the model of Burridge and Knopoff (1967) and its modifications "blocks" were understood as elements of the fault surface engaged in elastic interaction, in the IIEPT models the notion of a "block" is an idealisation of crustal blocks.) These models give an opportunity to carry out integral quantitative analysis of slow motions of an entire tectonic region and to study dependence of the earthquake flow on geometry of the fault system. They were employed in the study of seismicity of artificial regular block structures (e.g. of the "brick wall" type, see Gabrielov *et al.* 1986, 1989, 1990, and of a square region paved with square blocks of the same or different sizes, see Maksimov & Soloviev, 1996; Keilis-Borok *et al.* 1997; Rotwain & Soloviev, 1998), as well as of structures reflecting geometry of certain actual tectonic regions (see Gabrielov *et al.* 1993; Gasilov *et al.* 1995, 1996; Sobolev *et al.* 1996; Panza *et al.* 1997; Garianova & Rotwain, 1998; Soloviev & Rundquist, 1998; Rundquist & Soloviev, 1999; Ismail-Zadeh *et al.* 1999). While synthetic catalogs obtained by application of these models to certain regions (see Gasilov *et al.* 1996; Sobolev *et al.* 1996; Panza *et al.* 1997; Garianova & Rotwain, 1998; Soloviev & Rundquist, 1998; Rundquist & Soloviev, 1999; Ismail-Zadeh *et al.* 1999) mimic well some general patterns of observed seismicity, such as the Gutenberg-Richter law, reproduction of more subtle features of spatio-temporal clustering of earthquakes (including the presence and statistical distribution of foreshocks and aftershocks) remains problematic.

In order to reproduce fine statistical properties of real earthquake catalogs, one should take into account various physical processes responsible for the observed patterns of seismicity. A missing element in the "dry" tectonic fault models is fluid, migrating along faults. Importance of this factor in seismic processes is indisputable. However, the integral influence of fluids on tectonic processes is complex and not sufficiently well understood so far. The goal of the present work is to study migration of fluids through the faults network and to explore its implications for the seismic regime of a tectonic region.

On the one hand, fluids are known to be one of the major factors in the crustal dynamics, because they control the strength of crust (see Keilis-Borok, 1990a, 1994; Gabrielov & Newman, 1994) via two distinct mechanisms: The first one is purely mechanical and is based on the fact that fluid transmits pressure to the pore space. The second one is of physico-chemical nature (see Scholz, 1990). The impact of fluids on geotectonic processes is delivered via such nonlinear effects as, for instance, decrease of the permeable medium strength with an increase of pore pressure; degradation of friction strength of rocks in the presence of fluids; stress corrosion or Rhebinder effect (i.e. loss of strength of solids in contact with some surface-active liquids); chemical interaction with rocks. The nonlinearity can be strong; the effects may act on fast time scales and they are associated with important mechanical instabilities of lithosphere. For instance, rheological weakening can be responsible for rock strength reduction by a factor up to a million within several years (see Keilis-Borok, 1990a). Hence, fluids play a significant role in diverse processes of earthquake preparation and triggering (see Nur & Booker, 1972; Nur, 1973; Johnson *et al.* 1974; Segall & Rice, 1975; Rice & Simons, 1976; Ben-Zion, 1990; Nikolaevskii, 1990, 1996; Rice, 1992; Yamashita, 1997; Miller *et al.* 1999). Numerous phenomena involving fluids and reflecting the state of crust have been documented, some of which can potentially be useful for earthquake prediction (see reviews Roeloffs, 1988, 1996).

On the other hand, characteristic time scales of migration of fluids are intermediate between those of tectonic motion of blocks and seismic waves. An analytical modelling of fluid filtration along a system of "dry" and "wet" porous blocks constituting a plain fault (see Barenblatt *et al.* 1983) has shown that propagation of the

critical fluid pressure occurs with the speed comparable to the speed of migration of earthquake epicenters along faults. Similarity of the velocity of propagation of swarms' precursors and that of fluid diffusion was found in seismicity observations (see Caputo, 1992). Thus consideration of fluids is important for explanation of long-range interaction. (While action at a distance can be regarded as a consequence of the assumption that the entire crust is in a self-critical state (see Scholz, 1991), and it can be modelled by cellular automata approximation of interaction of an array of slider blocks (see Turcotte, 1997), consideration of a specific physical mechanism (or mechanisms) responsible for this phenomenon makes the model more realistic.) It can be important for replication of the characteristic spatio-temporal grouping of seismic events in the model.

2 A two-dimensional mathematical model of the Earth core block structure, involving fluid filtration through the faults network.

Our model (also discussed by Zheligovsky & Podvigina, 2002) is based on the assumption that the lithosphere can be regarded as a complex hierarchical block structure (see Alekseevskaya, 1977; Sadovsky *et al.* 1982, 1984; Sadovsky & Bolkhovitinov, 1990; Keilis-Borok, 1990a,b, 1994; Gabrielov & Newman, 1994). Blocks are separated by relatively thin and less consolidated transition zones, such as tectonic faults and lineaments, where most earthquakes occur. In what follows these interblock transition zones are indiscriminately referred to as "faults". These concepts are idealised: blocks are considered in the model as absolutely rigid two-dimensional polygons interacting via elastic forces, which act on their one-dimensional boundaries. Each fault is interpreted as a one-dimensional porous medium, along which filtration of fluids is possible. Fluids can proliferate to adjacent or crossing faults. A stress drop (interpreted as an earthquake) occurs when stress exceeds the strength at some point of a fault. This results in fast relocation of blocks, which can cause subsequent failures. Normal stress arising due to the relative displacement of blocks acts on the matrix of the porous medium, which causes variation of porosity and a build-up of fluid pressure gradients. Fluid pressure affects the motion of blocks

and weakens faults. As a result of an earthquake, fractures filled in with fluids can emerge in a fault. Fluid sources and sinks model production and consumption of fluids in geochemical processes. Phase transitions are not considered, fluids are supposed to be homogeneous and uniform, and thereafter we refer to them in singular. Porous medium is assumed to be saturated. Effects due to heat production and transfer are also neglected.

The model is comprised of equations of blocks motion, equations of fluid migration along the network of tectonic faults, criteria for triggering and termination of earthquakes, and formalisation of their impact on the block system. Our model is a generalisation of the model of Gabrielov *et al.* 1990.

Two time scales are introduced in the model: a geological time scale, on which slow tectonic motion of blocks takes place, resulting in accumulation of elastic energy and leading to earthquakes; and a seismic time scale, on which fast motion of blocks takes place during earthquakes, resulting in partial drop of the accumulated stress. The processes proceeding in slow time, namely tectonic loading and migration of fluids, are frozen in fast time.

2.1 Motion of blocks

Blocks are regarded as absolutely rigid polygons, which can move in horizontal directions and rotate about the vertical axis. (Implications of block rotation are discussed by Nur *et al.* 1989; Li *et al.* 1990.) Block boundaries are identified with fault segments. The density of each block is constant, it can vary for different blocks. The motion of blocks satisfies the Newton's law. Displacements of blocks are supposed to be infinitely small relative to their size, and equations of motion are linearised in displacements and in angles of rotation. The motion of blocks is caused by prescribed motion of the boundary blocks confining the tectonic block structure.

Denote the center of mass of the i-th block by $(X_i^c,\ Y_i^c)$. Let $\mathbf{r}_i = (x_i, y_i)$ be the vector of displacement of the center of mass of the i-th block and let ϕ_i be the angle of rotation of this block about the vertical axis. Displacement of the i-th block at a point (X, Y) is

$$\Delta_i(X, Y) = (x_i - (Y - Y_i^c)\phi_i, y_i + (X - X_i^c)\phi_i).$$

Dissipation of energy in the system is modelled by "viscous" forces, proportional to the rate of displacement. The density of the viscous force acting on the i-th block is

$$\mathbf{q}_i(X,Y) = -\mu_i \frac{d}{dt}\Delta_i(X,Y).$$

Viscosity coefficients μ_i are supposed to be constant for a given block. Viscous damping must be introduced into the model to avoid the purely oscillatory kind of motion, which sets in if the motion of blocks is primarily controlled by elastic forces considered next. For very large blocks it may model, for instance, interaction of a block with the partially melted base.

We now discuss interaction of two blocks along their common fault segment. Two kinds of forces are considered: elastic stress and pore pressure. In the course of relative motion of natural blocks their mutual traction along the joint boundary causes deformation of the blocks and thus accumulation of elastic energy within their volumes. We introduce elastic forces to model this accumulation of energy.

Consider a fault segment, which is a boundary between the i-th and j-th blocks. Let $\mathbf{e}_t$ be a unit vector parallel to the fault segment, whose direction agrees with the clockwise orientation of the j-th block boundary, and let $\mathbf{e}_n$ be the unit outward normal to the j-th block. (Directions of $\mathbf{e}_t$ and $\mathbf{e}_n$ are reversed when the i-th and j-th blocks are interchanged.)

Consider a point (X,Y) at the common boundary between the i-th and the j-th blocks. Displacement $\Delta_{i,j}(X,Y)$ of the i-th block relative to the j-th block at this point is $\Delta_{i,j}(X,Y) = \Delta_i(X,Y) - \Delta_j(X,Y)$. In the model, this relative displacement results in elastic interaction of blocks. The density of the elastic force acting on the i-th block is

$$\sigma(X,Y) = \sigma_t \mathbf{e}_t + \sigma_n \mathbf{e}_n, \tag{1.1}$$

where

$$\sigma_t = -K_t(\Delta_{i,j} \cdot \mathbf{e}_t - \delta), \tag{1.2}$$

$$\sigma_n = -K_n(\Delta_{i,j} \cdot \mathbf{e}_n - sh). \tag{1.3}$$

Here K_t, K_n are elastic coefficients in the directions along the fault and normal to it, respectively; $\delta(X,Y)$ is unelastic displacement along the fault (these quantities are defined at the end of Subsection 2.3); $\sigma_n(X,Y)$ is normal stress in the fault;

$h(X,Y)$ is the relative width of fractures filled in with fluid (see Subsection 2.2); s is a scaling factor; and $\sigma_t(X,Y)$ is tangent stress. For simplicity, elastic coefficients K_t and K_n are supposed to be constant at each fault segment, but they can vary for different segments. $\sigma_n > 0$ corresponds to compression, and $\sigma_n < 0$ – to extension. These equations are valid for in the elastic (non-broken) state of the fault; we call this state *basic*.

The contribution of the elastic force σ and the pore pressure p is weighted by the porosity m of the fault medium. (Constitutive laws governing the values of porosity are considered in the next section). Thus, the density of the total force acting on the i-th block at the point X, Y of the fault, is $\mathbf{f}(X,Y) = (1-m)\sigma + mp\mathbf{e}_n$.

Motion of the i-th block in slow time satisfies the Newton's law (see e.g. Landau & Lifshitz 1976):

$$M_i \frac{d^2}{dt^2}\mathbf{r}_i = \mathbf{F}_i, \qquad \mathcal{I}_i \frac{d^2}{dt^2}\phi_i = \mathbf{M}_i, \tag{2}$$

where

- M_i is the mass of the i-th block;
- $\mathcal{I}_i$ is the moment of inertia of the i-th block about the center of mass;
- $\mathbf{F}_i$ is the total force acting on the i-th block:

$$\mathbf{F}_i = \int_{\partial B_i} \mathbf{f}(X,Y)dl + \int_{B_i} \mathbf{q}(X,Y)\,dxdy$$

(integration is over the block boundary in the first integral, and over the area of the block in the second one);

- $\mathbf{M}_i$ is the total angular momentum of forces acting on the i-th block about the center of mass.

2.2 Fluid migration along the network of faults

Each fault segment is regarded as porous medium, which can be fractured. Conditions for opening and closure of fractures in the model will be discussed in the next subsection. Porous and fractured media are characterised by different values of the porosity m_i and permeability k_i ($i = 1$ for the porous, and $i = 2$ for the fractured medium).

Migration of fluid along the fault segment satisfies the Darcy's law (see Kochina, 1962; Nikolaevskii *et al.* 1970; Bear, 1972; Barenblatt *et al.* 1972, 1983, 1984; Fyfe

et al. 1978; Basniev *et al.* 1993; Nikolaevskii, 1996):

$$w = -\frac{k}{\nu}\frac{\partial p}{\partial l}. \tag{3}$$

Here w is the rate of filtration; k is the total permeability of the fault: in the absence of fractures $k = k_1$ is permeability of the porous medium, if fractures are open $k = k_1 + k_2$; ν is the fluid viscosity; l is the natural parameter on the fault segment (i.e. the distance from a point on the segment to one of the endpoints); p is the pore pressure (in the presence of fractures, fluid pressure in the fractures is equal to the pore pressure).

Constitutive equations for k, m, ν and fluid density ρ must be specified. The simplest relations were considered, in order to avoid artificial effects due to excessive complexity of the assumed governing relations, as well as to simplify computations. The following empirical relations have been assumed (see Nikolaevskii, 1996):

$$k_i = k_{i,0}(m_i/m_{i,0})^d,$$

where m_i is porosity of porous ($i = 1$) or fractured medium ($i = 2$).

$$m_1 = m_{1,0}e^{-\alpha_m(1-m_1)\sigma_{\text{eff}}} \tag{4.1}$$

(here

$$\sigma_{\text{eff}} = \sigma_n - p + \bar{p} \tag{5}$$

is effective normal stress, $\bar{p}$ is a normalisation constant, equal to the average initial pore pressure; it can be also regarded as representing compressive load in the model),

$$m_2 = h/(1 + h) \tag{4.2}$$

($h = 0$ initially and when there are no fractures; $h > 0$ is interpreted as the width of fractures relative the width of the unfractured fault zone; for fractured medium, porosity (4.2) due to fractures is defined in line with the general definition as the ratio of the volume of fractures to the total volume);

$$\nu = \nu_0 e^{\alpha_\nu p}; \qquad \rho = \rho_0 e^{\alpha_\rho p}$$

Here $d, \nu_0, \rho_0, k_{i,0}, m_{i,0}, \alpha_\nu, \alpha_\rho, \alpha_m$ are constants. Power laws with $d = 2$ or 3 were considered for permeability. Constants $k_{i,0}, m_{i,0}, \alpha_m$ can vary for different fault segments, but for the sake of simplicity they are not supposed to depend on the point of a segment.

Filtration of fluid satisfies the mass conservation law

$$\frac{\partial}{\partial t}((m_1 + h)\rho) + \frac{\partial}{\partial l}(\rho w) = Q,$$

where $Q(l,t)$ is the prescribed rate of fluid production or consumption in a source (respectively, sink) at a point l of the fault. Following Barenblatt *et al.* (1972, 1983), substitute here the rate of filtration (3) to obtain a nonlinear parabolic partial differential equation for the pressure p:

$$\frac{\partial}{\partial t}((m_1 + h)\rho) = \frac{\partial}{\partial l}\left(\rho \frac{k}{\nu}\frac{\partial p}{\partial l}\right) + Q. \tag{6}$$

Boundary conditions at a point of the fault intersection or junction express the continuity of pressure and the mass conservation for the fluid passing through the point. Consider a point of intersection or junction of several fault segments. For the i-th fault segment, for which it is an endpoint, let l_i denote the natural parameter on the segment, $l_i = 0$ being this endpoint. Then the boundary conditions take the form

$$\lim_{l_i \to 0} p(l_i) = \lim_{l_j \to 0} p(l_j) \quad \forall i, j \tag{7.1}$$

(continuity of the pore pressure when passing from the i-th fault segment to the j-th one; note that this implies under our assumptions that the fluid density is also continuous);

$$\rho \sum_i w_i|_{l_i=0} = q \tag{7.2}$$

(mass conservation for the fluid passing through the point). Summation is carried out here over all fault segments which end at this point, w_i is the rate of filtration on the i-th fault segment, and $q(t)$ is the prescribed rate of fluid production/consumption at the point.

Some points can be assumed to be attached to unlimited basins of fluid with a prescribed dependence of pressure on time $p_b(t)$. At such points the condition

$$p = p_b(t). \tag{7.2'}$$

is therefore satisfied instead of (6) or (7.2). All such points are regarded as endpoints of fault segments.

2.3 Seismic events

The fault segment retains its elastic properties as long as certain strength thresholds are not exceeded. We introduce two conditions for the elastic behaviour, based on Coulomb's law (see Kasahara, 1981; Scholz, 1990):

$$\sigma_{\text{eff}} > -C \tag{8.1}$$

$$|\sigma_t| < A\sigma_{\text{eff}} + B \tag{8.2}$$

Here C is the extension strength threshold; A and B determine the shear strength threshold. (The three constants are positive, they can vary for different fault segments.)

When elastic stress at a fault segment exceeds the medium strength, i.e. (8.1) or (8.2) are violated, a seismic event resulting in stress drop is registered in the model (cf. with Gabrielov *et al.* 1990). The slow time processes are frozen, and the fast time motion of the system begins. We consider two kinds of failures: extension fracture, occurring when σ_{eff} is negative, and shear rupture, occurring when it is positive.

Extension fracture. At the part of the fault segment where $\sigma_{\text{eff}} < 0$, fractures emerge and they are filled in with fluid. After this elastic stress vanishes, and henceforth

$$\sigma_{\text{eff}} = \sigma_t = 0. \tag{9.1}$$

Shear rupture. At the part of the fault segment where $\sigma_{\text{eff}} > 0$, slip along the fault begins. The effective normal stress remains unaffected, and the tangent stress is replaced by dynamic friction, so that at the broken part of the segment

$$|\sigma_t| \leq a\sigma_{\text{eff}}. \tag{9.2}$$

Here a satisfies $0 \leq a \leq A$. It is assumed to be constant on each fault segment.

Direction and magnitude of σ_t in the regime of dynamic friction is determined from the following conditions. Consider the tangent component of the relative displacement rate,

$$\mathbf{v}_t = \frac{d}{dt}\Delta_{i,j}(X,Y)\cdot\mathbf{e}_t. \tag{10}$$

If $\mathbf{v}_t \neq 0$, the magnitude of dynamic friction is set to the maximum possible value, $|\sigma_t| = a\sigma_{\text{eff}}$, and the sign of σ_t is opposite to the sign of $\mathbf{v}_t$. Otherwise ($\mathbf{v}_t = 0$), friction is determined from the requirement that it sustains (10), or if the upper bound (9.2) is too small to make this possible, its direction is against the relative acceleration of blocks at this point due to the action of all other forces, and its magnitude is set to the maximum permitted value. (Note, that if (10) holds on several fault segments, the values of σ_t must be determined from the respective set of equations. This is considered in more detail in section 2.4 .)

Regime of dynamic friction terminates at the end of the earthquake (conditions for which will be defined below), or when the fault opens, $\sigma_{\text{eff}} < 0$, whichever happens first.

The change of stresses, discussed above, causes motion of blocks in fast time. In the beginning of an earthquake zero velocities of the fast time motion are assumed. The motion of blocks in fast time satisfies the second Newton's law (2), where $\mathbf{F}_i$ and $\mathbf{M}_i$ are the sums of the following forces and their moments:

• elastic stress σ, calculated from (1) for the parts of fault segments in the basic elastic state, and from (9) for the parts of fault segments in broken states of either kind;

• the force of viscous dissipation of energy in the block

$$\mathbf{q}(X,Y) = -\mu_i^e \frac{d}{dt}\Delta_i(X,Y),$$

where μ_i^e is the viscosity coefficient, which can be different from the slow time viscosity coefficient;

• pore pressure p of the fluid, which is determined during an earthquake at every point from the condition that the local content of the fluid remains constant (fluid migrates only on the slow time scale), taking into account (1.3), (4) and (5). This translates to

$$m_1\rho = const, \tag{11.1}$$

if the fault is not open ($\sigma_{\text{eff}} > 0$); otherwise, p and h are determined from the conditions (9.1) and

$$(m_1 + h)\rho = const. \tag{11.2}$$

Due to fast time relocations of blocks, stress changes. Consequently, the strength threshold (8) can become surpassed at parts of fault segments which have not yet failed, or effective normal stress σ_{eff} can change sign. The new failures are treated in the same way, as the ones which have failed at the beginning of an earthquake. If σ_{eff} becomes positive at any point where the fault is open, it closes and the regime of dynamic friction sets in.

The fast time motion of blocks continues till the system arrives to an equilibrium state. After it is reached, the earthquake is declared to have terminated, and faults heal everywhere, where they failed but did not open. Unelastic displacements δ along the fault, constant in the slow time, are reset, so that the new tangent stress (1.2) equals tangent stress σ_t at the equilibrium: $\delta = \Delta_{i,j} \cdot \mathbf{e}_t - \sigma_t / K_t$. (Initially unelastic displacements are set to zero.)

An earthquake magnitude M is determined as[1]

$$M = M_0 + \log_{10} \int \delta E dl, \tag{12}$$

where M_0 is a normalisation constant, integration is performed over all failed parts of fault segments, and δE is the elastic energy drop,

$$\delta E = (\Delta^+ - \delta^+ \mathbf{e}_t) \cdot \sigma^+ - (\Delta^- - \delta^- \mathbf{e}_t) \cdot \sigma^-$$

(the superscript $-$ refers to the quantities just before the beginning of an earthquake, and the superscript $+-$ to those just after its end). An alternative magnitude M' is also considered, also defined by (12), where however integration is performed over the entire faults network. The point, where the initial failure happened at the beginning of an earthquake, is regarded as its epicenter.

After an earthquake ends, the slow time evolution of the system resumes from the positions at the end of the earthquake, and with the velocities at the end of the slow time motion right before the earthquake. If σ_{eff} becomes positive on an open fault during this evolution, the fault heals, and non-elastic displacement δ is calculated from the condition that the tangent stress (1.2) vanishes: $\delta = \Delta_{i,j} \cdot \mathbf{e}_t$.

[1]For real earthquakes $M = M_0 + \frac{2}{3} \log_{10} E$. However, since the model is two-dimensional, it is natural to assume a unit coefficient in front of the logarithm.

2.4 Numerical algorithms

Spatial and temporal discretisation.

Each fault segment is divided into a number of intervals of equal (for a given segment) length, not exceeding a prescribed threshold ϵ. These intervals are referred to as "cells", and their endpoints – as "nodes". In particular, endpoints of all fault segments are nodes. All physical fields are evaluated at nodes. The partitioning is employed for the spatial discretisation in (6), integration of forces and moments in (2), and examination of conditions for failure (8). Epicenters are also defined in terms of nodes: the node which failed at the start of an earthquake represents its epicenter (if several such nodes failed, the one with the maximum stress drop is selected).

Finite differences (see Gear, 1971; Press, 1992) are used for the solution of differential equations (6) and (2). First derivatives in the first term at the r.h.s. of (6) are obtained at the centers of cells by a standard rule: if a cell is defined by the inequality $l_0 \le l \le l_1$, then

$$\frac{\partial p}{\partial l}\left(\frac{l_0+l_1}{2}\right) = \frac{p(l_1)-p(l_0)}{l_1-l_0}. \tag{13}$$

Since discrepancy of this formula is quadratic in $|l_1 - l_0|$, the values can be used for evaluation of the second derivative at nodes by the same rule. However, we use a slightly different scheme, which guarantees conservation of the total fluid mass in a closed fault network.

Let a "fluid cell" be defined as a subinterval of a fault segment between the centers of two adjacent cells (hence the center of a fluid cell is a node). From (13) and the Darcy's law (3) one obtains filtration rates at the endpoints of a fluid cell, and hence finds the balance of fluid in the cell (taking into account the rate of fluid production/consumption Q). Assuming constant rates of fluid filtration through boundaries of the fluid cell during a time step, and normalising the variation of fluid content by the length of the fluid cell, calculate the fluid content $m\rho$ at the center of the fluid cell at the next moment of time. This procedure is equivalent to the use of a second order spatial finite-difference scheme for (6).

Discretisation of the boundary condition (7.2) for (6) guarantees conservation of

the total fluid mass migrating through segment endpoints. Consider a node which is an intersection or junction of two or more faults, and define a fluid cell, with the center at the node, as the union of all half-cells adjacent to this node. One finds the rate of filtration from (13) and (3) and determines the balance of fluid in the cell (taking into account the rate of fluid production/consumption q at the central node). Assuming that the rates of fluid filtration through the boundaries remain constant during the time step, and normalising the variation of the fluid content by the total length of half-cells constituting the fluid cell under consideration, one finds the fluid content at the central node at the next moment of time.

Computational scheme.

Suppose all the quantities are known. The following operations are carried out to make the next time step:

1. Integrate (2) to find new positions of blocks and their velocities.

2. In slow time: integrate (6) to find fluid content (11) at every internal (non-boundary) node at the new moment of time.

3. Using boundary conditions (7), find fluid content at every boundary node.

4. Calculate new relative displacements of blocks at each node.

5. Using (1), (4) and (11), calculate new values of normal stress, pore pressure, fluid density and porosity at each node.

6. At each open node check the condition of closure of fractures $\sigma_{\text{eff}} > 0$. If it is satisfied, assume the basic elastic state of the node at slow time following healing, or assume dynamic friction at fast time; hence, reevaluate normal stress, pore pressure, fluid density and porosity, and at slow time – the non-elastic displacement δ.

7. In fast time at each node in the state of dynamic friction check the condition of fault opening $\sigma_{\text{eff}} \leq 0$. If it is satisfied, assume this state of the node, assign a zero value to normal stress, and reevaluate pore pressure, fluid density and porosity.

8. Calculate new tangent stress at each node taking into account its state (using (1.2) or (9)).

9. At each node (except for those in the state of dynamic friction at fast time) check the condition (8) of failure. If it is satisfied, in slow time declare an earthquake and switch to fast-time computations. Determine the types of occurring failures and

reevaluate the values of stress from (9), as well as of pore pressure, fluid density and porosity.

10. At fast time check the condition of termination of an earthquake (i.e. that block velocities, total forces and moments acting on each block do not exceed prescribed thresholds) If it is satisfied, find the new non-elastic displacements δ at all nodes which are in the state of dynamic friction, and return to computation of the slow time evolution.

Determination of dynamic friction forces.

To determine dynamic friction in (9.2) we employ the following procedure. Assuming all forces to be constant one can find the time interval $dt' > 0$, after which the tangent component of the relative displacement rate will vanish at the first of the nodes in the state of dynamic friction. If dt' is less than the standard time step dt, then the Euler's time step of the length dt' is made. (This test is performed at each time step, while nodes in the state of dynamic friction exist.) Suppose the condition (10) is satisfied at N nodes. The following heuristic algorithm is used to determine the forces of friction at these nodes:

0. Find the upper bounds F_i (the r.h.s. of (9.2)) for the friction forces. The index i refers to nodes where the friction forces have to be determined.

1. Construct the system of equations in unknown friction forces f_j. An equation for the i-th node expresses the condition that the tangent acceleration along the fault vanishes; it is of the form

$$\sum_{j=1}^{N} \ell_i^j f_j = \xi_i. \tag{14}$$

Since necessarily $\ell_i^i \neq 0$, without any loss of generality assume $\ell_i^i > 0$.

2. If for some index i

$$\xi_i > \sum_{j=1}^{N} |\ell_i^j| F_j,$$

then $f_i = F_i$; if

$$\xi_i < -\sum_{j=1}^{N} |\ell_i^j| F_j,$$

then $f_i = -F_i$. Substitute these values to the remaining equations and return to step 1 for the reduced system of equations.

3. If the system of equations splits into several independent subsystems, each one is treated separately.

4. Find a solution $\tilde{f}_i$ to the reduced subsystem (14). If $|\tilde{f}_i| \le F_i, \ \ \forall i$, go to step 6.

5. Find (and store) the index i, for which the ratio $|\tilde{f}_i|/F_i$ is maximum, and set $f_i = F_i \mathrm{sign} \tilde{f}_i$. Substitute this value to the remaining equations and return to step 1 for the reduced system.

6. If all friction forces f_i assigned at step 5 are directed opposite to the acceleration along the fault at the respective nodes, the solution for the subsystem is obtained.

7. Discard all the values assigned at step 5 and consider the original independent (sub)system of equations, before step 5 was applied for the first time. Construct for it an auxiliary system of ordinary differential equations

$$\frac{d\phi_i}{d\tau} = \gamma_i \left(\xi_i - \sum_{j=1}^{N} \ell_i^j \phi_j \right), \tag{15}$$

where

$$\gamma_i = F_i - \phi_i, \ \text{if} \ \xi_i > \sum_{j=1}^{N} \ell_i^j \phi_j;$$

$$\gamma_i = F_i + \phi_i, \ \text{if} \ \xi_i < \sum_{j=1}^{N} \ell_i^j \phi_j.$$

By construction, the steady state of this dynamical system is a solution to the problem, possessing all required properties.

8. Solve (15) numerically. In case this step is performed for a given subsystem for the first time, assume zero initial conditions; otherwise continue the trajectory. Due to the presence of factors γ_i at r.h.s. of (15), $|\phi_i| < F_i$ for all $\tau > 0$. Since a solution of the original problem was not obtained at step 5, $\lim_{\tau \to \infty} |\phi_i| = F_i$ for at least one index i. As soon as the inequality $F_i - |\phi_i| < \epsilon$ is satisfied for some i, stop solving (15) and set $f_i = F_i \mathrm{sign} \phi_i$ for this index; substitute this value to the remaining original equations (14) and apply steps 1-6 to the reduced system. Here ϵ is a prescribed small positive number; its value is decreased each time when we return to this step for the given subsystem.

In practice, one needs to solve (15) very rarely, and thus the algorithm allows to determine unknown friction forces fast.

3 Results of simulations for the "brick wall" structure

We considered a two-dimensional model of an artificial regular block structure, shown on Fig.1. The top and bottom confining blocks are moving with the same constant speed in opposite directions (the upper block to the right, and the lower one to the left; here and in what follows directions "up", "down", "left" and "right" refer to the orientation of Fig.1). The left and right confining blocks are rotating clockwise with the same constant angular velocity coherently with the motion of the top and bottom confining blocks. The faults adjacent to confining blocks are called external; all other faults are internal. This is the so called "brick wall" block structure, studied by Gabrielov *et al.* 1990.

Initially the pore pressure p and the fluid content $m\rho$ are the same at all nodes. Four variants of simulations were carried out, different in the fluid boundary conditions:

(a) fluid is locked in a closed faults network;

(b) the faults network is connected to an unlimited basin of fluid at a constant pressure, equal to the initial one, at the upper left and lower right corners;

(c) a constant pressure gradient is maintained: the faults network is connected at the upper left corner to an unlimited basin of fluid at a constant pressure, equal to the initial one, and at the lower right – to another unlimited basin at a smaller constant pressure;

(d) no fluid is present.

Diagrams, labelled on Figures by (a)-(d), refer to the 4 variants, respectively. Each of these simulations require more than a week of CPU time of a DEC Alpha workstation.

The following constants, same for all fault segments, were used in the reported simulations: $M_0 = 4, D = 2, \alpha_m = 0.005, \alpha_\nu = 10^{-4}, \alpha_\rho = 10^{-5}, \mu = 0.1, \mu^e = 0.5, K_t = 0.6, K_n = 1, a = 0.1$. The values of constants, defining strength threshold, are the same as in Gabrielov *et al.* 1990: $A = 1, B = 0.5, C = 0.5$. A power law with $d = 2$ is assumed for permeability. The horizontal side of each full-size block is cut into 20 cells, and of each of the 3 blocks of the half-size – into 10 cells; each

vertical side – into 6 cells. All cells are of the same size. Simulations at an interval of 2000 time units are performed. The assumed constants scale up to tectonic blocks of the 200 km $\times$ 60 km size, the cell length (and hence the precision of the epicenter location) 10 km, the time unit is of the order of several years, relative velocity of motion of the upper and lower confining blocks 1 cm/year. No important differences were found in the behaviour of the block system in additional simulations with a twice finer spatial discretisation (of the same structure with the same values of constants) at an interval of 1000 time units.

Fig.2 illustrates the simulated earthquake flow. There are 1177, 3200, 5768 and 2226 events with $M \geq 4$ in the synthetic catalogs for the variants (a)-(d), respectively. Temporal behaviour of the structure is non-stationary in all variants (at least on the considered time interval), perhaps except for (c). In the variant (a) average seismicity is monotonously increasing, although the flow of strong earthquakes may have saturated and become stationary. In variants (b) and (d) locally maximum magnitudes grow in time. This growth may be related to compression in horizontal direction, which each layer of blocks experiences due to rotation of the vertical confining blocks, and in variants (a)-(c) – also with the peculiarities of the fluid regime.

The magnitude M, used on Fig.2, correlates for $M > 4$ (or $M > 5$ in variant (a)) with M', and at these magnitude intervals $M \approx M'$ (see Fig.3; $M' > M$ for large M). There is no correlation of the magnitudes for small seismicity. Since the motion of blocks is coherent, in most cells the amount of the stored elastic energy decreases during a seismic event. and hence in most cases $M' > M$. In large events the number of cells, broken during the event, is large. Moreover, the fast-time motion of blocks is large in amplitude, causing to break many cells with initially a subcritical amount of elastic energy. Thus only those cells remain unbroken, where a small amount of elastic energy is stored, and their number is relatively small. This explains why $M' \approx M$ for large events.

The magnitude M is employed in what follows. Graphs of the released seismic energy (Fig.4) are similar for variants (b) and (d). Their parabolic shape also indicates non-stationarity of seismic flows on the considered time interval.

In variants (b)-(d) the Gutenberg-Richter law $\log_{10} N(M) \approx -\alpha M + \beta$ is satisfied with α =0.7–0.8 (Fig.5). A non-regular shape of the histogram in variant (a) and the minor value of the coefficient α in the remaining variants can be related to non-stationary of the simulated earthquake flows.

Figs. 6-10 illustrate spatial distribution of epicenters in synthetic catalogs. The cell length serves as a unit for the x coordinate along the horizontal axis, i.e. labels of axes on the Figures display the number of nodes along a horizontal fault. Histograms of pairs (x_i, x_{i+1}) of horizontal coordinates of epicenters of all consecutive earthquakes are shown (Fig.6), as well as histograms of pairs of consecutive earthquakes at each horizontal fault (Fig.7-10). The number of pairs at a given cell of a histogram is gray-scale coded (zero pairs – white color, the maximum number – black color).

Two classes of regions of an increased density of distribution of the pairs of epicenters can be seen on Fig.6: (1) horizontal and vertical lines corresponding to the values of x_i and x_{i+1}, which are multiples of 10, and (2) two subdiagonal lines $|x_i - x_{i+1}| = 1$. Clustering of the first class is related to a well-known fact that epicenters tend to be located near points of faults intersection or junction. The second class reveals the spatial correlation of consecutive earthquakes: the next earthquake tends to occur in a node adjacent to the one where the previous earthquake has occurred. These patterns persist if a sequence of earthquakes with epicenters on a given horizontal fault is considered (with the exception of internal horizontal faults in the variant (d) where the number of earthquakes is very small), as well as if earthquakes with $M \geq 4$ are considered, though in this case clustering of pairs (x_i, x_{i+1}) near the diagonal is less pronounced. The degree of earthquake clustering in the aforementioned regions varies for different variants, and it is less pronounced for the internal horizontal faults than for the external ones. This can be attributed to the fact that in all variants the number of earthquakes on internal horizontal faults is smaller than the number of those on the external horizontal faults.

In variants (b) and (d) inhomogeneity of the earthquake locations is noticeable. There were practically no earthquakes at the bottom fault with epicenters in the

intervals $x_i \leq 5$ and $76 \leq x_i \leq 99$ (Fig.7), and at the top fault – in the intervals $7 \leq x_i \leq 26$ and $x_i \geq 102$ (Fig.10). This can be explained by a common pattern of collective motion of blocks. Displacements and rotations of individual blocks are exaggerated on Fig.11 (as a result, blocks near vertical boundaries are displaced one relative to another in the horizontal direction). Respective diagrams for variants (c) and (d) are not shown, since they are visually identical to Fig.11 (b).

The same kinematic mechanism is responsible for the same pattern of displacements of blocks in all variants. Due to rotation of the right confining block, the upper part of the right external vertical fault opens, implying that normal stress acting on the upper rightmost block vanishes there, which causes clockwise rotation of that block. Similarly, all blocks near vertical boundaries rotate in the clockwise direction. This causes compression and relocation of internal blocks. As a result, layers take an S-shape form. Consequently, the upper horizontal external fault opens in the left part, and the lower horizontal external fault – in the right part, and therefore zones of seismic quiescence emerge on these faults. Thus earthquakes happen in the quiescence zones only in the beginning of the evolution of the block structure.

Non-stationarity of the seismic flow can be attributable to this pattern of collective motion of blocks. As the time goes on, layers of blocks increasingly bend. This causes an ongoing increase of normal stress at the places of contact of the top and bottom layers with the top and bottom confining blocks. Consequently, the growing strength thresholds make it possible to sustain increasing tangent elastic stress. The latter are growing due to the motion of the confining blocks. This results in a steady increase of maximum magnitudes in time. Thus, the observed non-stationarity of seismicity is related to geometric incompatibility (see Gabrielov *et al.* 1996) of block motions. In natural block systems it is controlled by the strength of blocks: when it is exceeded, blocks break with emergence of new transverse faults. Collapse of blocks is not allowed in the present model.

Qualitative dissimilarity in the observed seismicity patterns and in displacements of blocks in (a) and in the three other variants owes to difference of their fluid regimes. Rotation of the left confining block causes compression in the left external vertical fault near upper vertices of adjacent internal blocks, and formation of

fractures filled in with water near lower vertices. The same kinematic mechanism acts near the right external vertical fault: fractures filled in with water emerge there near upper vertices of blocks. Fluid, concentrating in these pockets, is partly pressed out of inner vertical faults due to compression of layers of blocks in the horizontal direction by the left and right confining blocks. In variants (b) and (c) it is also sucked in from the unbounded basins, to which the network of faults is attached (by the end of simulations the total amount of fluid in the faults system is about twice larger in (b) and (c), than the initial one; in (b) it is larger, than in (c)). These effects are of course not found in variant (d) with no fluid (which is equivalent to a constant pressure). Since in variant (a) the total amount of fluid is conserved, its outflow to pockets near vertical external faults causes an overall decrease of pressure in the faults system; hence fluid pressure in the pockets is less capable to compensate moments of normal stress exerted on blocks of the structure by the left and right confining blocks. This results in larger angles of rotation of blocks in this variant, than in the remaining three. Variant (a) is also distinct in the following respect: An overall decrease of pressure is equivalent to increase of strength thresholds. For this reason an average number of earthquakes of magnitude above a certain level per unit time is smaller in (a), than in other variants, and the average magnitude is higher (see Fig.2).

Large negative normal stresses appeared in virtually all runs for the model brick wall structure near the blocks which have rotated most, near the left and right boundaries (see Fig. 11). They are unphysical and suggested introduction of tensile fractures into the model, though normally no natural earthquakes of this type occur. Being artificial, with a large number of orthogonal faults, geometry of the brick wall structure is apparently responsible for occurrence in the model of this unusual in seismology type of seismic events. Their number is not large: tensile fractures occur in the beginning of simulations at the faults, where relative angles of rotation of blocks are large, and the fractured faults do not heal in the subsequent evolution of the block system. Thus, they can be also regarded as representing an initial transitional stage of adjustment of the model – by contrast, natural faults in the Earth core evolve in the saturated regime.

4 Results of simulations for the Israeli seismic region

The block structure used in the model.

We have used in simulations a conventional pattern of the Sinai Subplate boundaries (see Salamon *et al.* 2003; Fig. 12). On the Figure one can see the Dead Sea Transform (DST), which accommodates the motion between Arabia and Sinai (northeastern tip of Africa), the convergent Cypriot Arc (CA) at the suture between Anatolia and Sinai, and the Suez Rift (SR), which carries some divergence between Africa and Sinai. While clearly these are plate boundaries, there is almost no morphological, tectonic or seismic evidence of the northward continuation of SR towards the CA, to completely encircle Sinai Subplate and define it as a microplate. Consequently, to model seismicity of the Sinai Subplate we have chosen an approximately triangular region with the Eastern boundary along the DST and the Southern boundary - along the SR. The western boundary of the selected block, crossing the Mediterranean Sea, passes by the epicenter of the 1997 ML=5.9 deep earthquake. Possibly the western boundary should be drawn further to the West, in accordance with the seismicity pattern which links Northern Africa with the Cyprian Arc. But in this case it is difficult to "close" intraplate blocks of the Sinai Subplate, corresponding to the Carmel-Fari'a (CA) tectonic system and the Negev Shear Zone, important for the area seismicity evaluations. According to the existing paradigm (see Ben-Menahem & Aboodi, 1981; Joffe & Garfunkel, 1987) Africa moves towards Anatolia at ~ 1 cm/yr (see Ginat *et al.* 1998). Arabia moves towards Anatolia with the velocity ~ 2.5 sm/yr. There is no consensus about the velocity of the Sinai Subplate itself. Long-term (on the scale of millions of years) indications suggest that the relative velocity of the shift between the Dead-Sea fault boundaries is ~ 1 cm/yr. Thus, the south-western boundary should move to the North-East with a 1.5 cm/yr velocity. Many GMT measurements were performed in the region in the last decade but no reports about the current plate motion velocity are yet available.

Other parameters used for computations are as follows. According to gravimetry and magnetic measurements (see Rybakov *et al.* 1999, 2002), the Sinai Subplate

density varies from 2.5 g/sm^3 at the upper crust to 3.3 g/sm^3 in the upper mantle. The Moho depth varies from 18 km to the West of the Dead Sea Fault to 35 km to the East, from 32 km in the South to 25 km in the North (see Ben-Avraham *et al.* 2002); the width of the Dead Sea Fault varies from 2 to 12 km.

Interpretation of results.

The model computations yielded a synthetic earthquake catalog (Time, Latitude, Longitude, Magnitude), which we compare to the real seismic catalog, compiled at the Geophysical Institute of Israel (GII) in 1981-2002. It was assumed in computation of the synthetic catalog that the system of faults was closed and it did not contain fluid sources or sinks. Figure 13 presents Magnitude/Time cross-section for the synthetic catalog. Almost stationarity of the catalog is evident. Maximum computed magnitude is $M = 6.1$.

The GII catalog events with $ML > 2.5$ between 1985 and 2002 selected for the rectangular area: latitude 27 - 38, longitude 32 - 36.5 are shown on Fig.14. The total number of events is 4694. The spatial distribution of the catalog events is shown on Fig.16 together with the main faults used in the simulated model. At least four prominent earthquake clusters can be seen: one is associated with the Cyprus Arc, the second with the Gulf of Aqaba, the third with the Suez Rift, and the fourth with the Dead Sea. In our model the Cyprus Arc was not present. Figure 17 demonstrates spatial density $P = dN/dS$ of events taken from the GII catalog. Figure 18 shows spatial density of the synthetic catalog. Inevitably, Figs. 17 and 18 have essential discrepancies. For example, the density maximum in the GII catalog corresponds to the Gulf of Aqaba area, while the density maximum of the synthetic catalog lies between the nodes corresponding to the NSZ-DST and CF-NST junctions. This happens because the seismic swarm of the Gulf of Aqaba cluster has a much higher (about 30 times) density than the overall (averaged) density of the region (excluding CA), and apparently this is not explained by the mechanisms, taken into account in our model. Thus, to make a sensible comparison of the two catalogs we filter out from the GII catalog all the CA events and resample the GA cluster so that only one event out of each thirty events remains. The remaining catalog is comprised of 1256 events (see Fig.19).

There are 2848 events with $M > 2.5$ in the synthetic catalog. Thus, intensity of the catalog is 2848/2000=1.424 events per time unit, while the GII catalog contains after filtering 1256 events, thus the intensity being 1256/18=70 1/yr. Hence, 50 time units in the synthetic catalog correspond to 1 year. A stationary 900 time units long synthetic catalog sample (the 500 - 1400 interval) equivalent to the 18 years long GII real catalog is shown on Fig. 15. On Fig.18 one can see that there are almost no significant events along internal faults. The maximum of the synthetic intensity is located between the latitudes 30 and 32 - the same as for the filtered GII catalog. Comparison of Figures 18 and 19 shows that there are still essential differences between the GII filtered catalog and the equivalent 900 time units long synthetic catalog. For example, the GII is more representative by magnitudes between 4 and 5, while the synthetic one has more events with $M > 5.5$ and $M < 3.5$ (see also Fig.20). Figure 20 shows the magnitude-number distribution of events in the GII and synthetic catalogs, which turns out to be essentially nonlinear. Roughly two branches can be selected in the GII distribution, with the Guttenberg-Richter b value being ~ 0.3 between magnitudes 2.5 and 4.5 and $b \sim 1.$ within the 4.5 - 6.5 interval. For the synthetic catalog $b \sim 0.6$ for magnitudes between 2.5 and 5.5 and $b \sim 0.15$ between magnitudes 5.5 and 6.5.

5 Conclusion

A detailed description of a two-dimensional mathematical model of a tectonic block structure, incorporating migration of fluids along tectonic faults, was presented together with the related numeric algorithms. Results of numeric simulations based on the model for an artificial regular "brick wall" block structure were reported for four variants differing in fluid regimes. Collective motion of blocks was found to be determined by geometry of the tectonic structure and by motion of confining blocks, and to be independent of fluid regime. Spatial clustering of epicenters was observed. Patterns of the simulated earthquake flows depended on the boundary conditions for fluid. A reasonable qualitative agreement of the simulated earthquakes catalog and the catalog of the Geophysical Institute of Israel is found in model simulations for the Israeli seismic region. However, the quantitative agreement is not very good. An

almost stationary synthetic catalog was obtained in seismometer-recordable range of magnitudes. Tuning simulation parameters, we obtained the maximum magnitude and the relative rates of occurrence in different magnitude ranges close to real values. However, large discrepancy remained. By filtering out the Cyprus Arc cluster and decimating the Aqaba cluster (they are caused by a mechanism not considered in the model) the spatial earthquake pattern was mimicked, as well as relative rates of occurrence of earthquakes of magnitude between 3 and 5. However, the number of the smallest $M \leq 2.5$ and the largest $M \geq 6$ events is yet almost two times greater than in the real catalog of the Geophysical Institute of Israel after filtering.

Acknowledgments

The research was supported by the INTAS-RFBR grant IR-97-1914 (RFBR grant 97-05-71092). The study was also partly made possible by the US Civilian Research & Development Foundation for the Independent States in the Former Soviet Union (CRDF) grant RG2-2237. We acknowledge financial support from the grant EAR 9804859 of the National Science Foundation, USA. The authors are grateful to the Referee Dr T.Yamashita for his valuable comments, which were very useful for improvement of the paper.

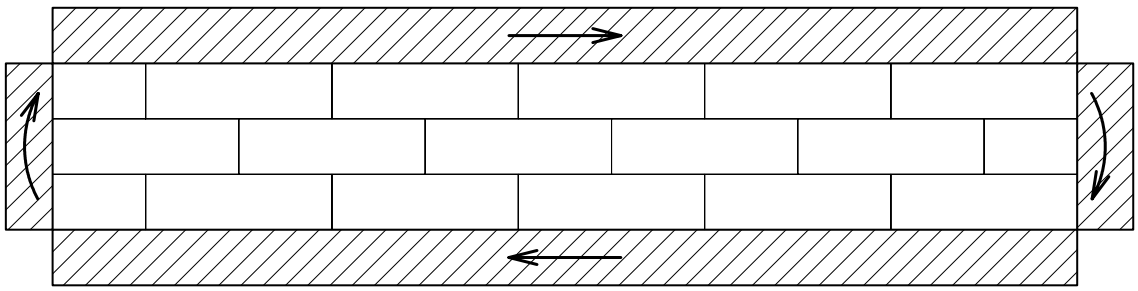

Figure 1. Geometry of the "brick-wall" block structure. Confining blocks are hatched. Directions of their motion are shown by arrows.

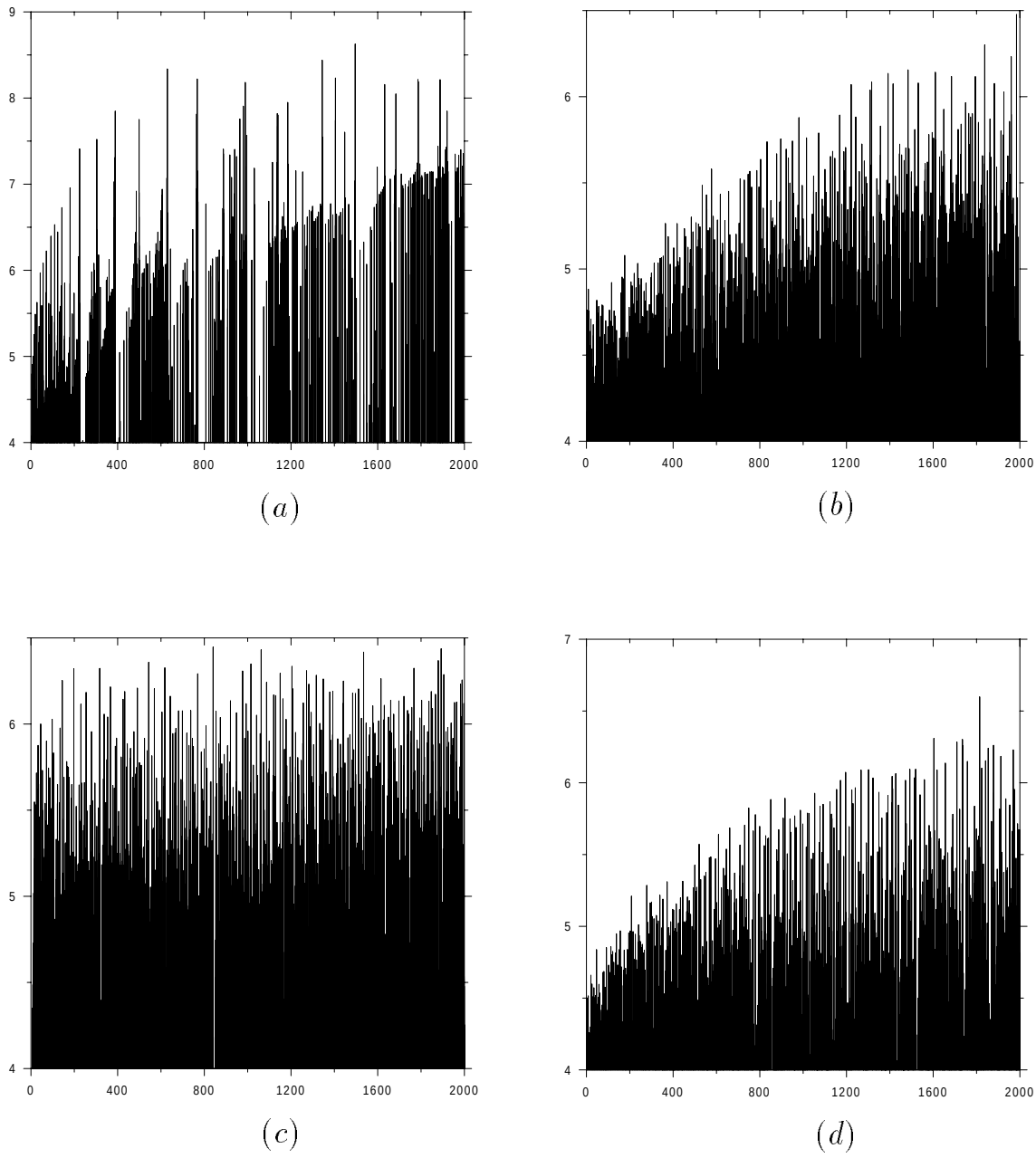

Figure 2. Earthquake flows for $M \geq 4$. Vertical axis: magnitude M of an event, horizontal axis: time of an event.

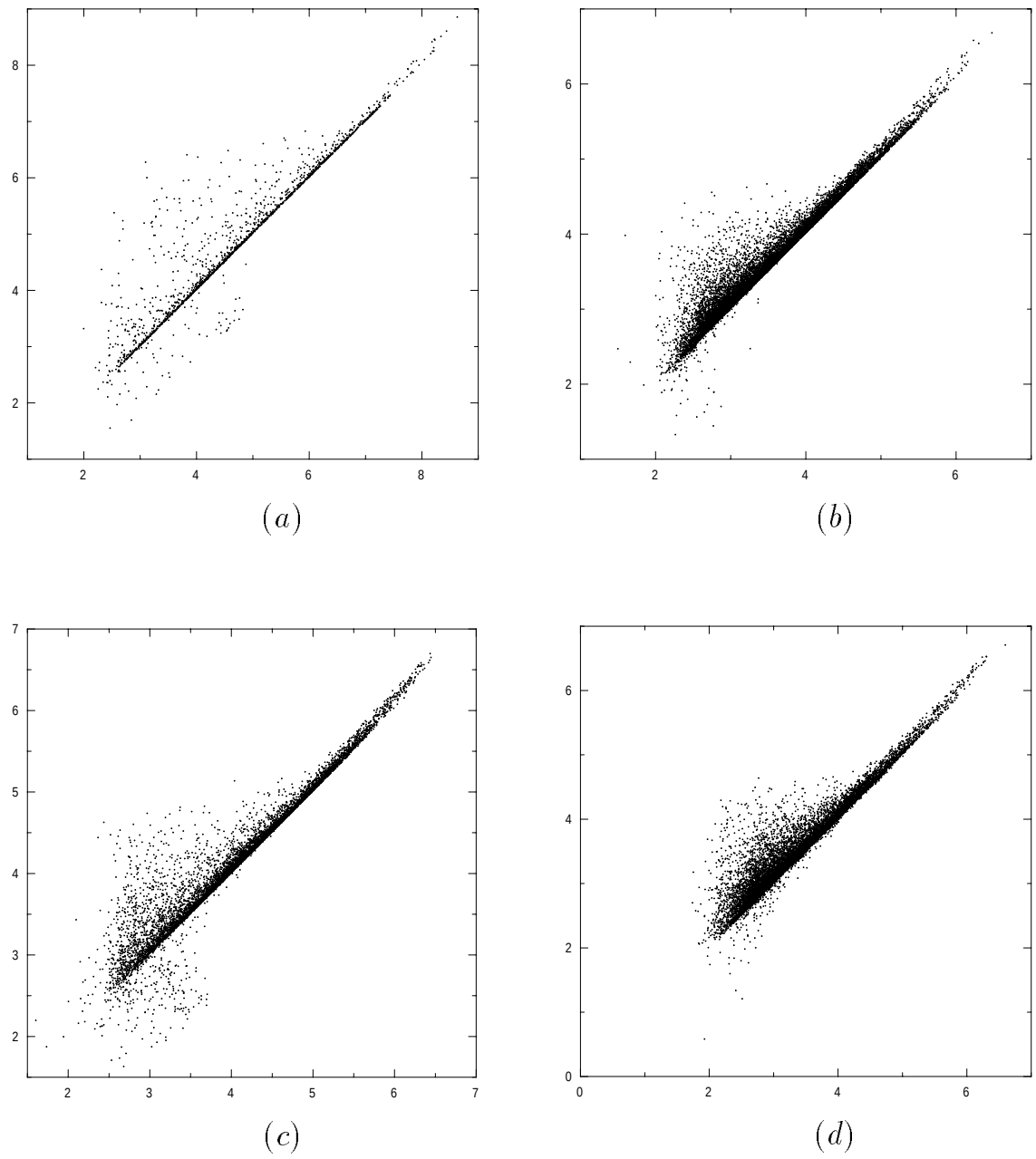

Figure 3. Correlation of magnitudes M (horizontal axis) and M' (vertical axis).

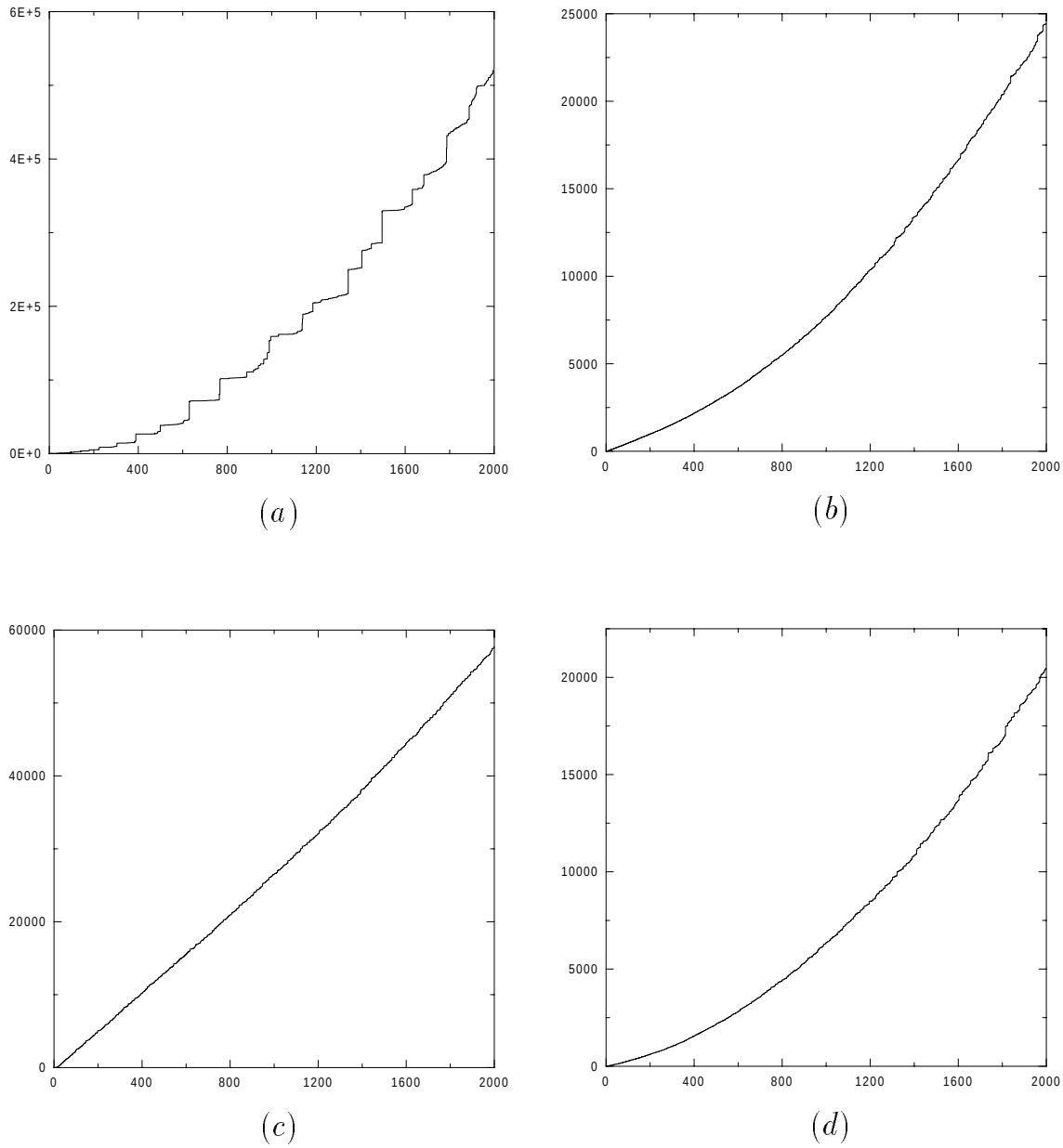

Figure 4. Simulated seismic energy release. Horizontal axis – time, vertical axis: released energy.

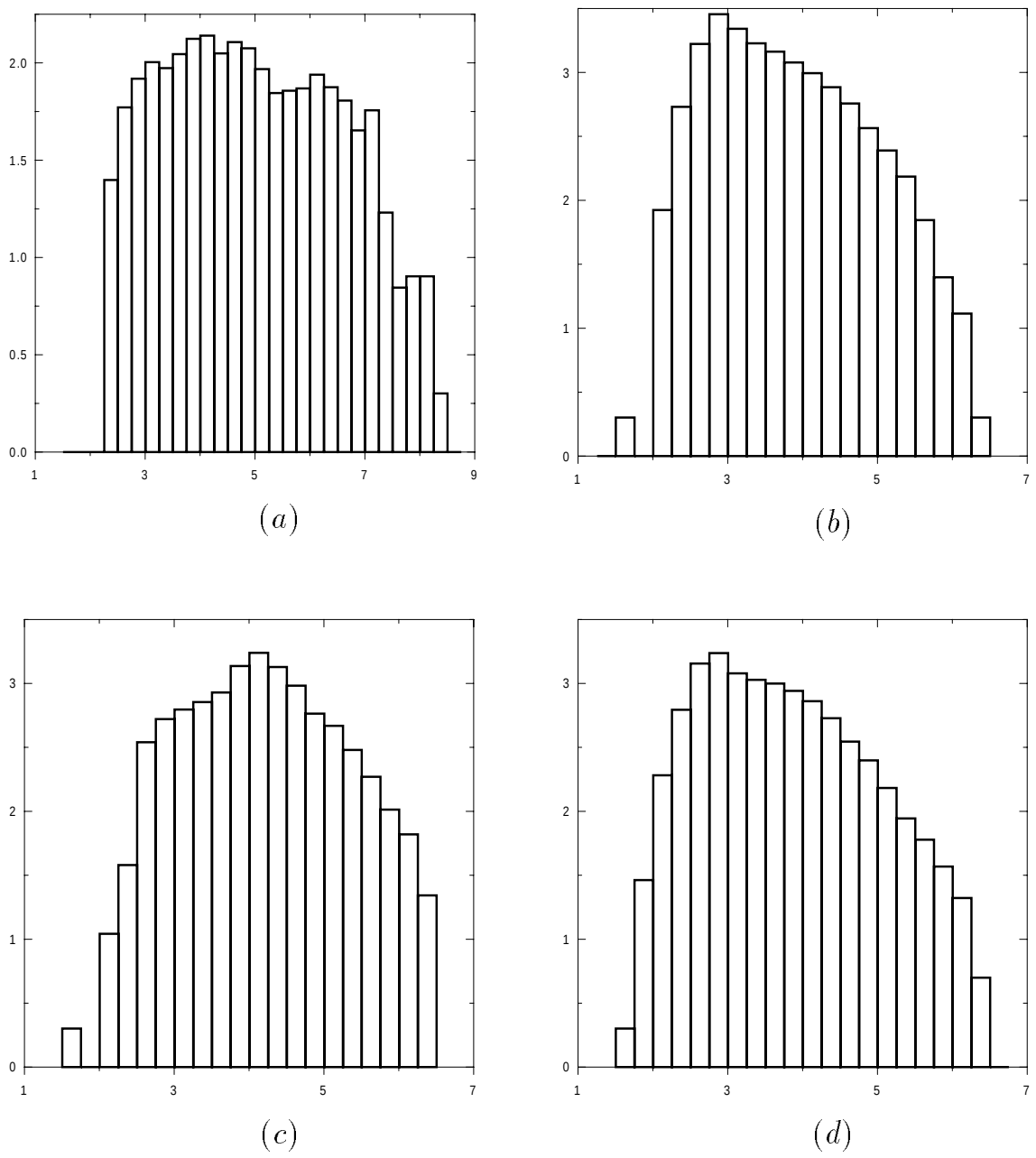

Figure 5. Histograms of the number of earthquakes in equal magnitude intervals. Vertical axis: $\log_{10} N(M)$, horizontal axis: magnitude M.

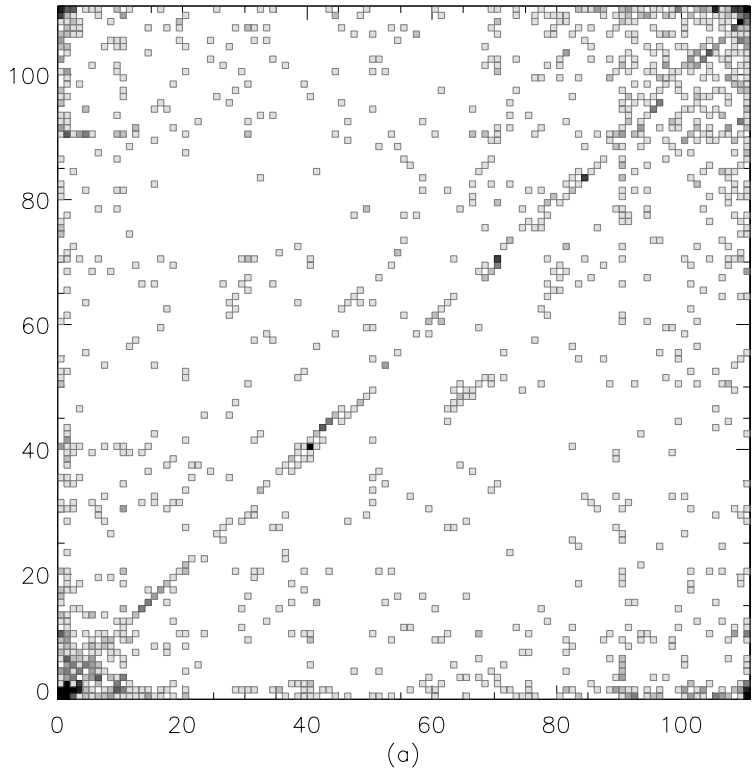

(a)

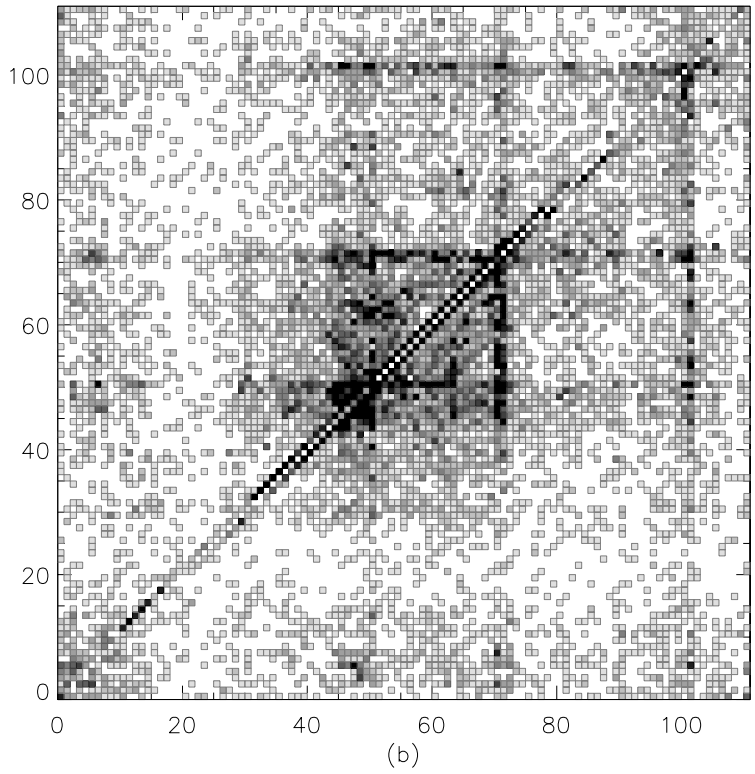

(b)

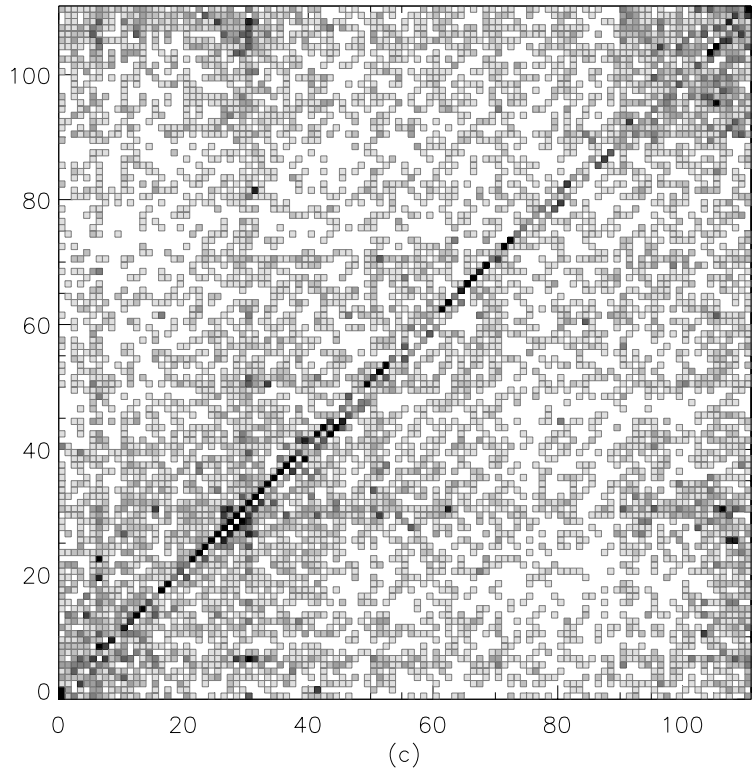

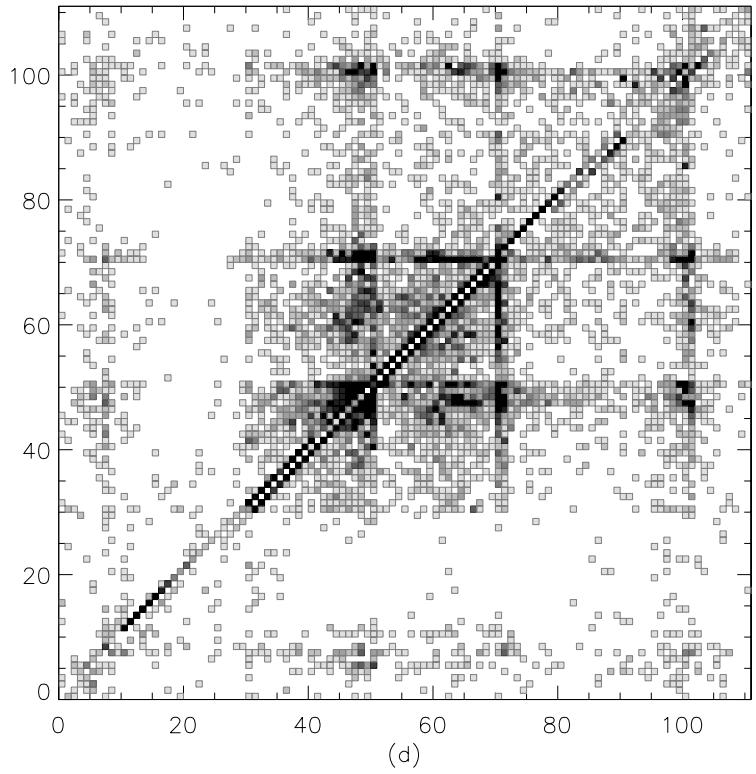

Figure 6. Histograms (gray scale coded) of the number of pairs of horizontal coordinates (x_i, x_{i+1}) of epicenters of consecutive earthquakes for entire synthetic catalogs. Horizontal axis: x_i, vertical axis: x_{i+1}.

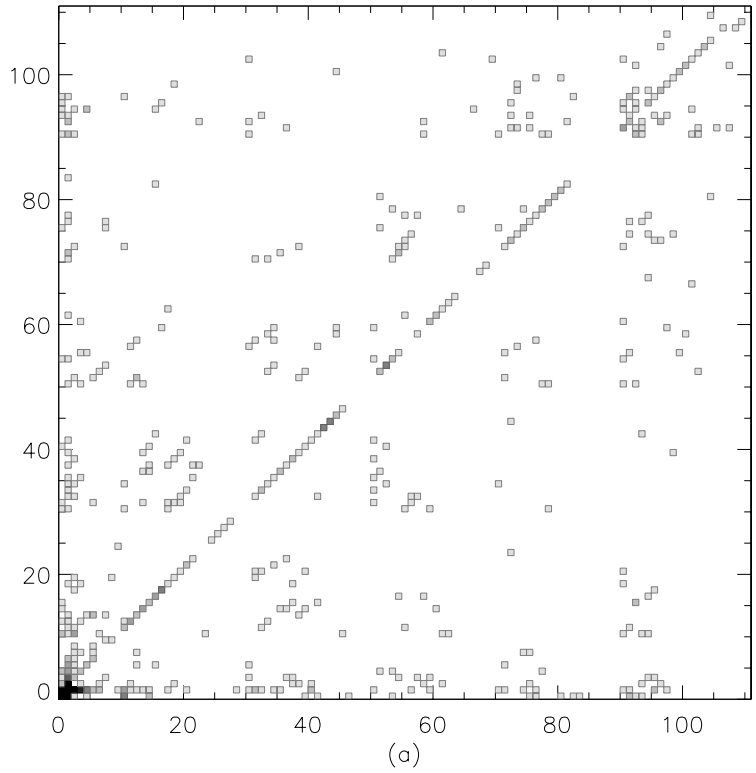

(a)

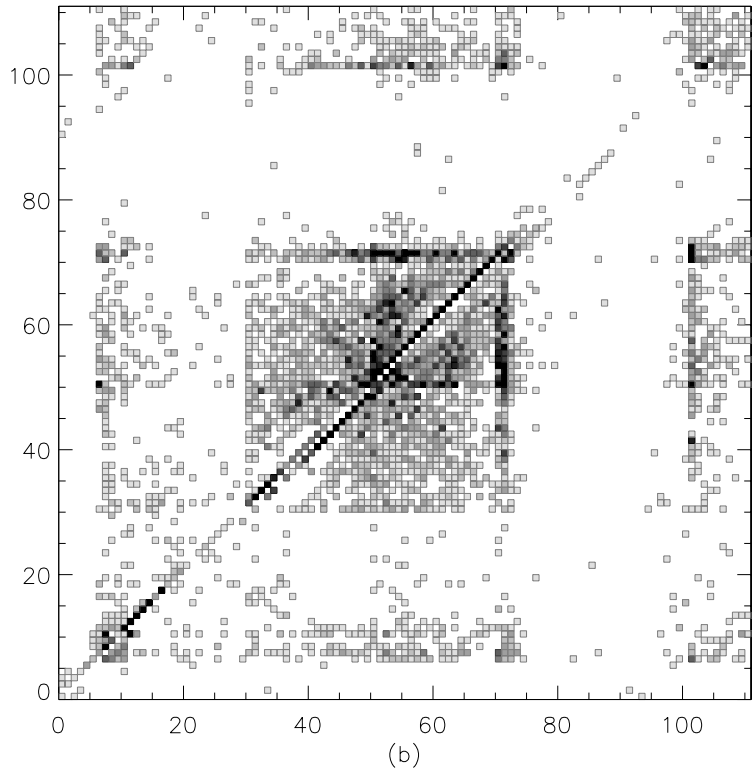

(b)

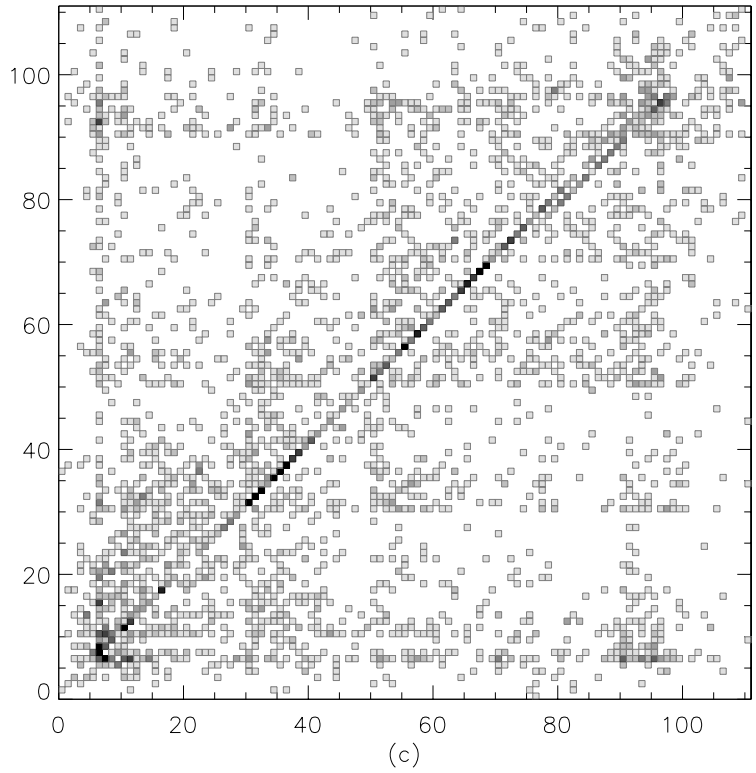

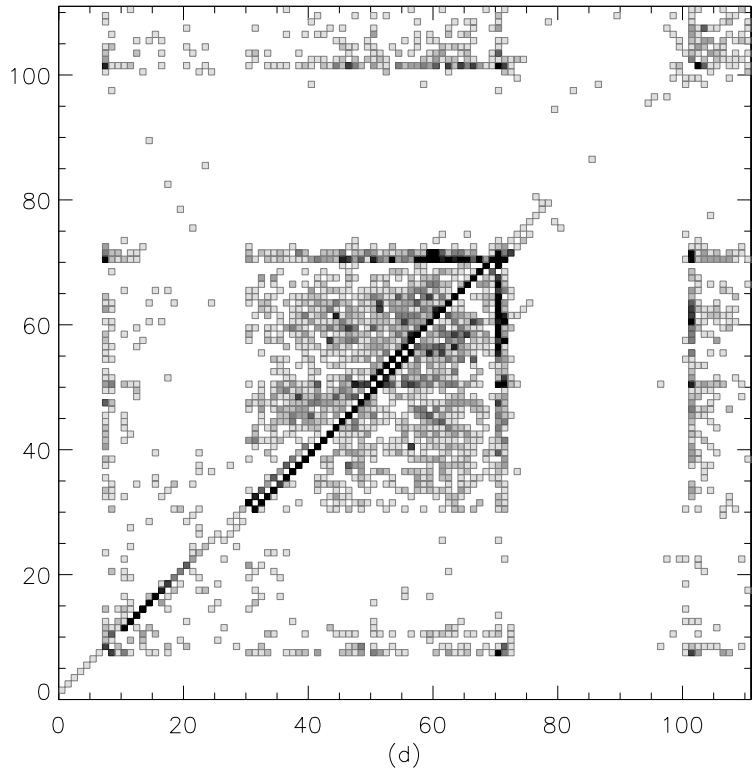

Figure 7. Histograms (gray scale coded) of the number of pairs of horizontal coordinates (x_i, x_{i+1}) for the epicenters of consecutive earthquakes, which occurred at the lower boundary of the tectonic region. Horizontal axis: x_i, vertical axis: x_{i+1}.

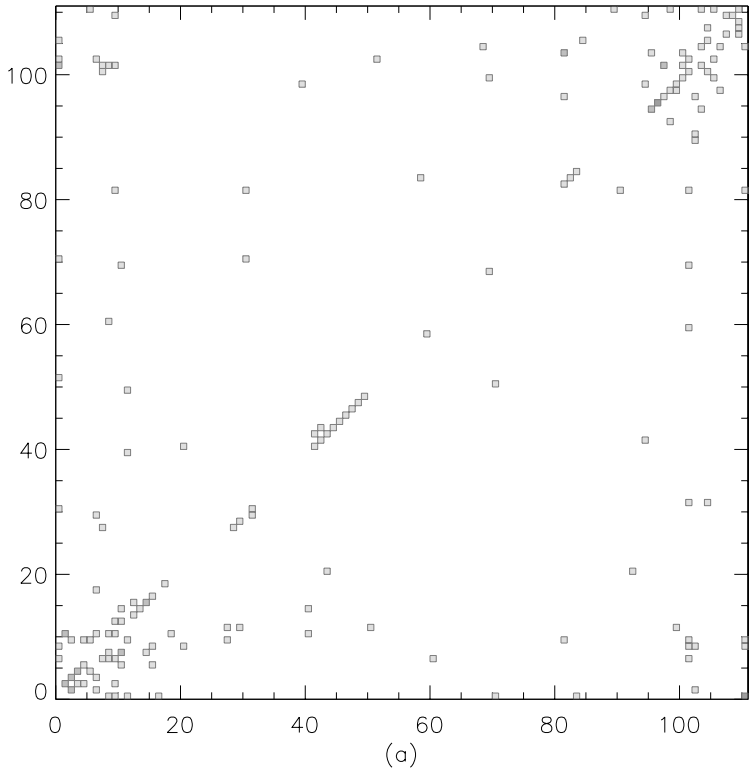

(a)

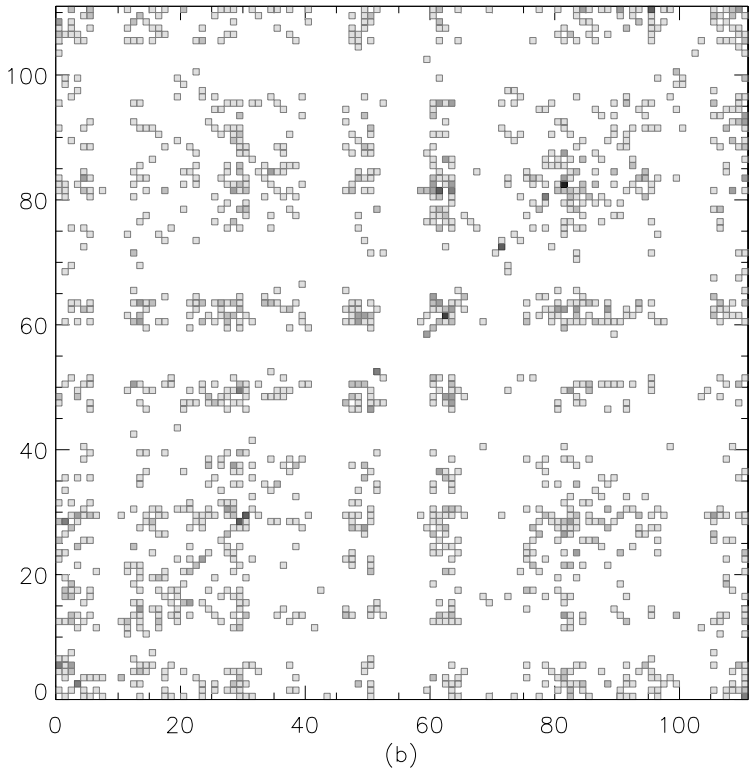

(b)

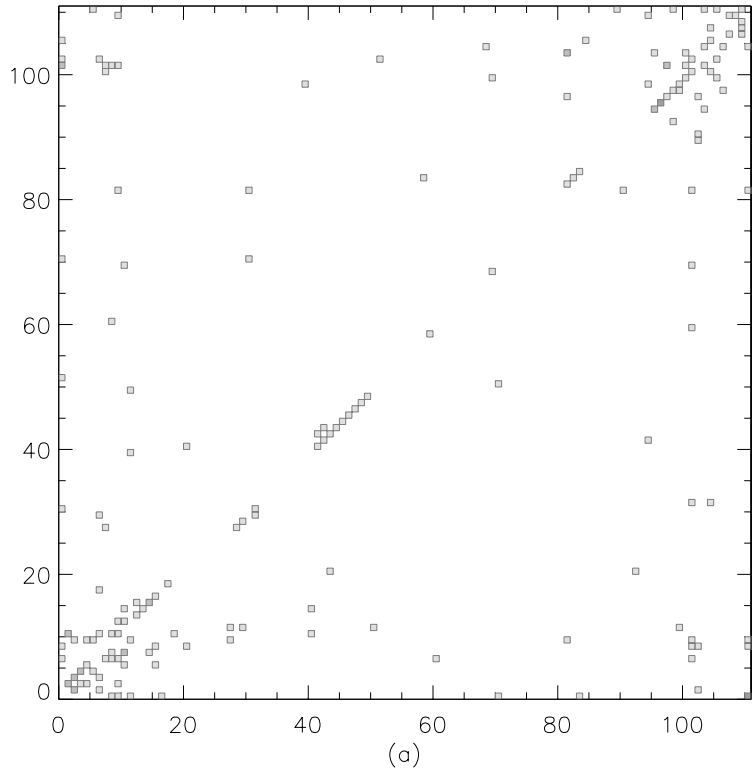

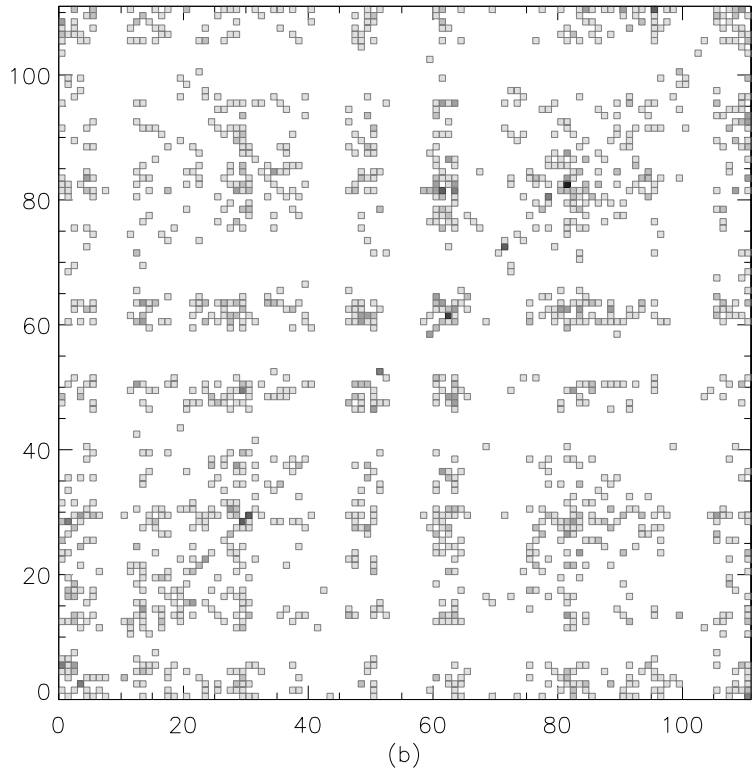

Figure 8. Histograms (gray scale coded) of the number of pairs of horizontal coordinates (x_i, x_{i+1}) for the epicenters of consecutive earthquakes, which occurred on the lower internal horizontal fault. Horizontal axis: x_i, vertical axis: x_{i+1}.

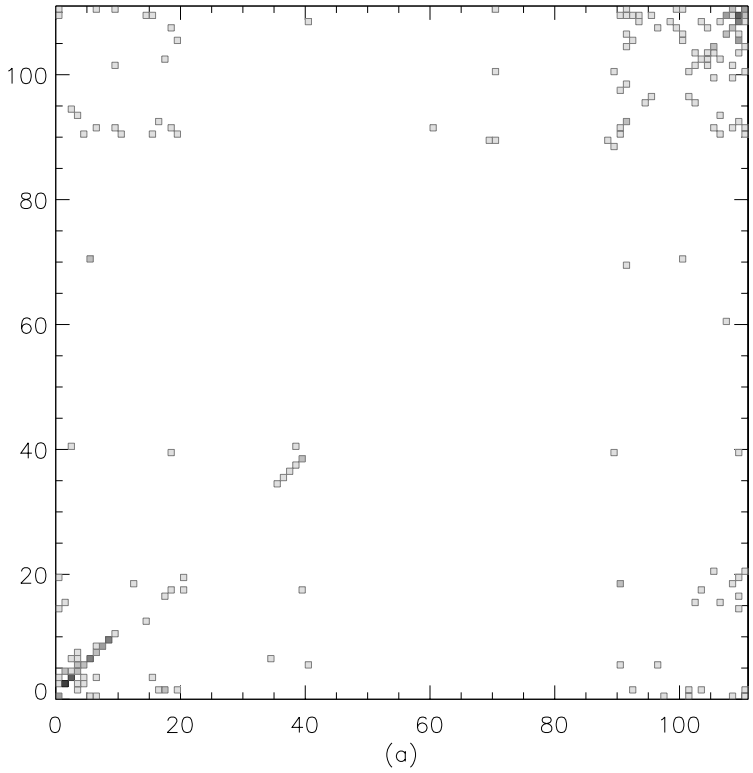

(a)

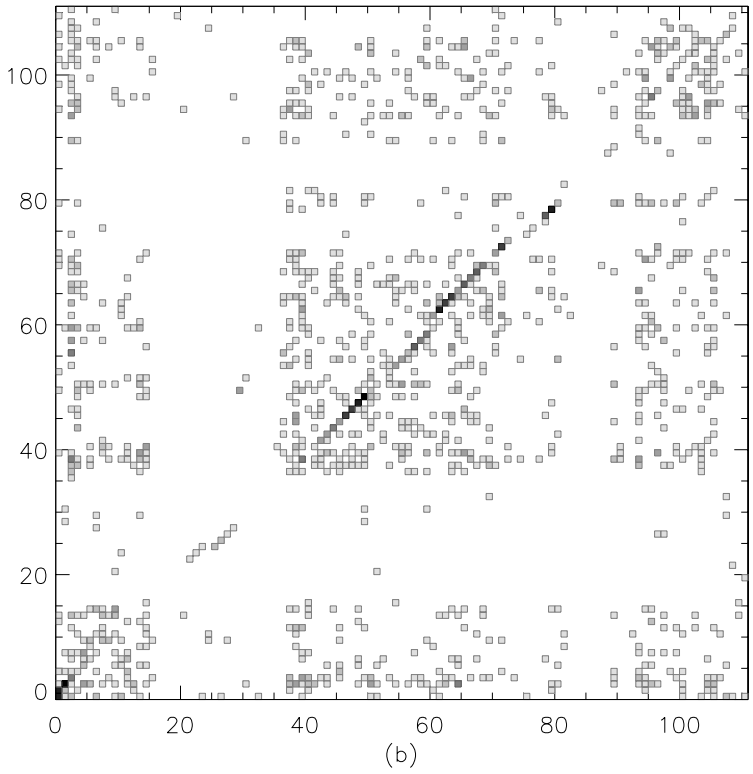

(b)

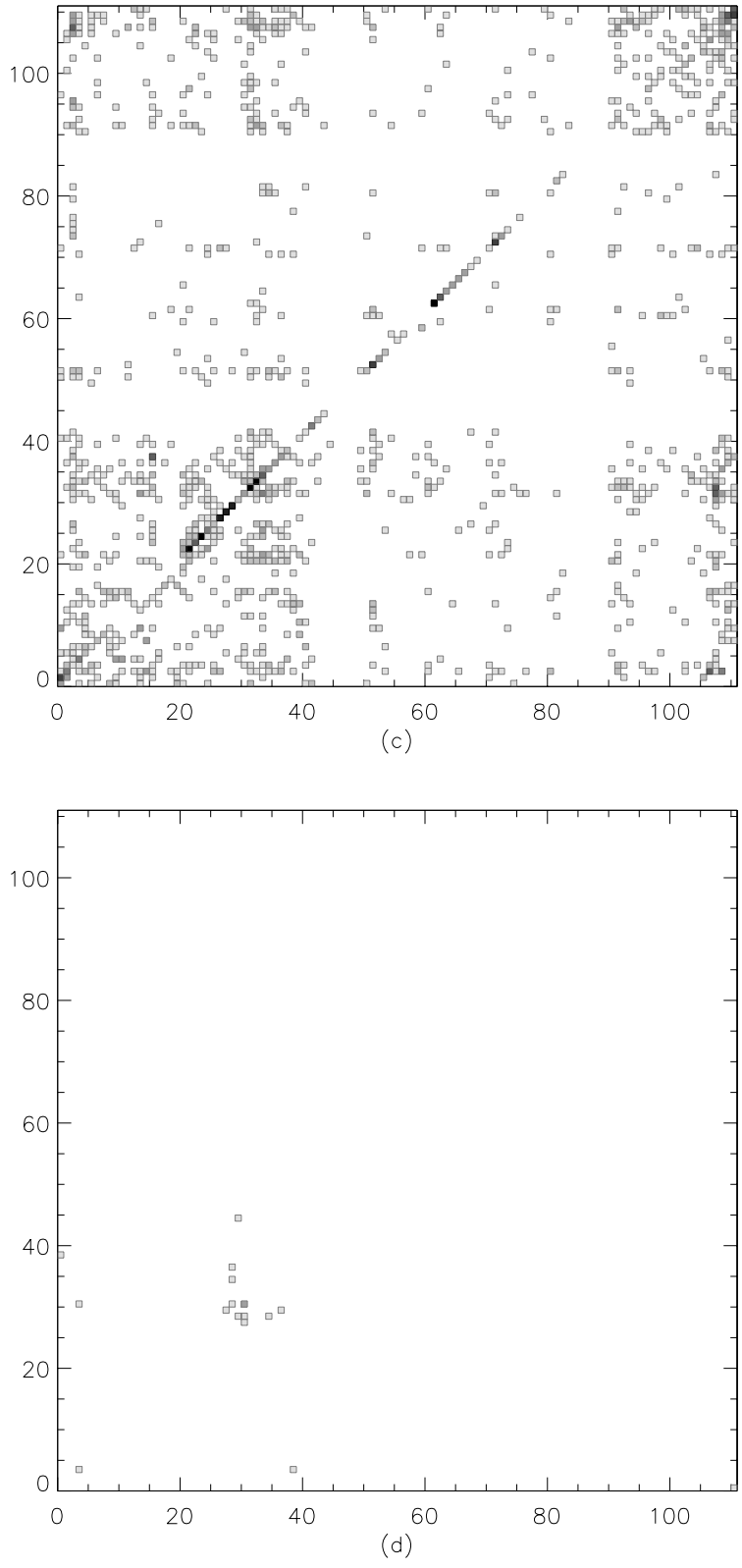

Figure 9. Histograms (gray scale coded) of the number of pairs of horizontal coordinates (x_i, x_{i+1}) for the epicenters of consecutive earthquakes, which occurred on the upper internal horizontal fault. Horizontal axis: x_i, vertical axis: x_{i+1}.

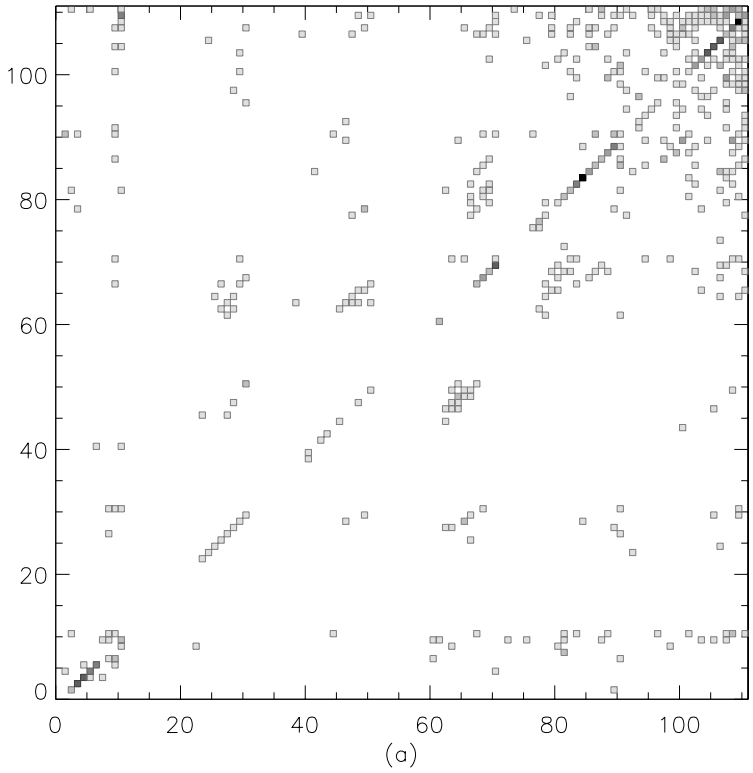

(a)

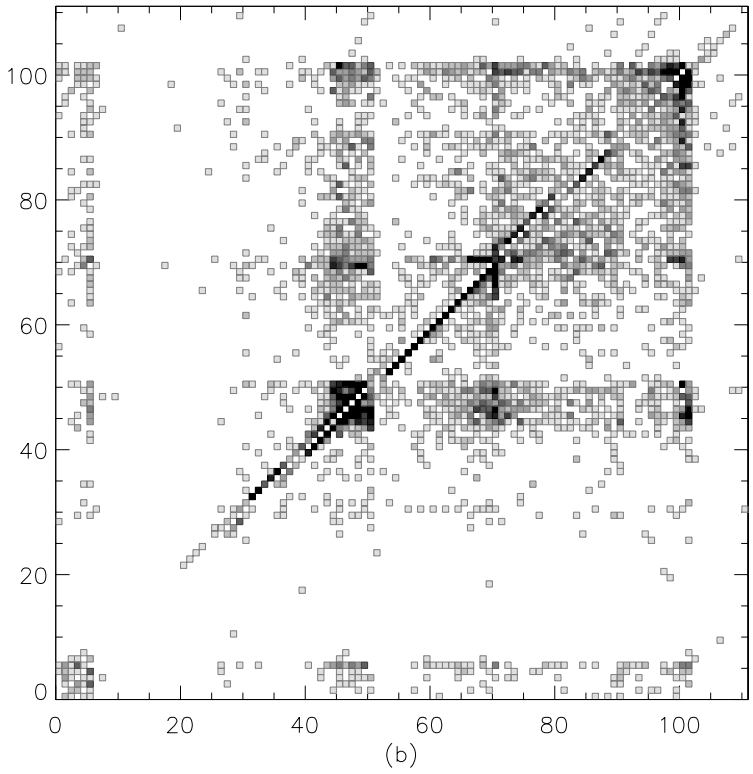

(b)

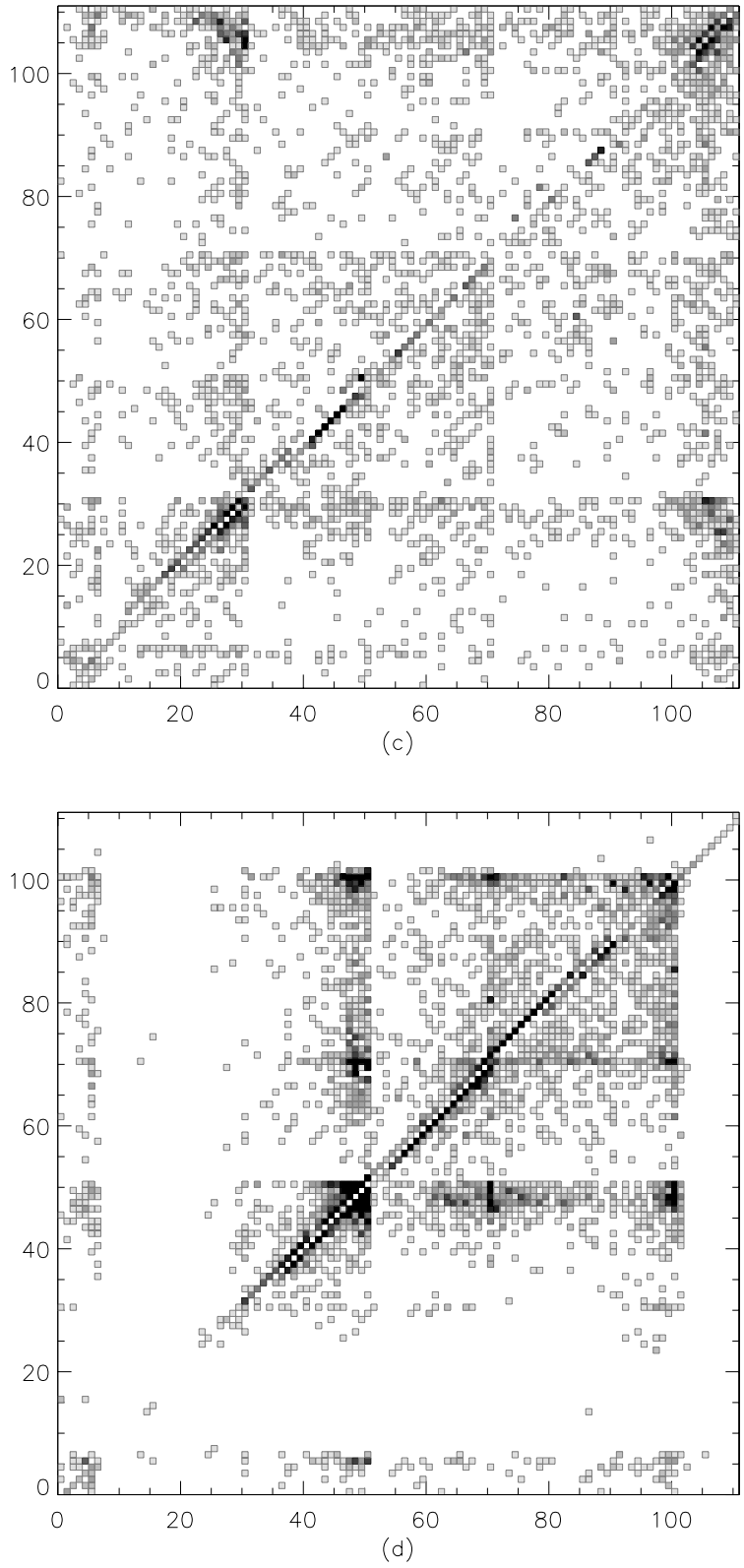

Figure 10. Histograms (gray scale coded) of the number of pairs of horizontal coordinates (x_i, x_{i+1}) for the epicenters of consecutive earthquakes, which occurred at the upper boundary of the tectonic region. Horizontal axis: x_i, vertical axis: x_{i+1}.

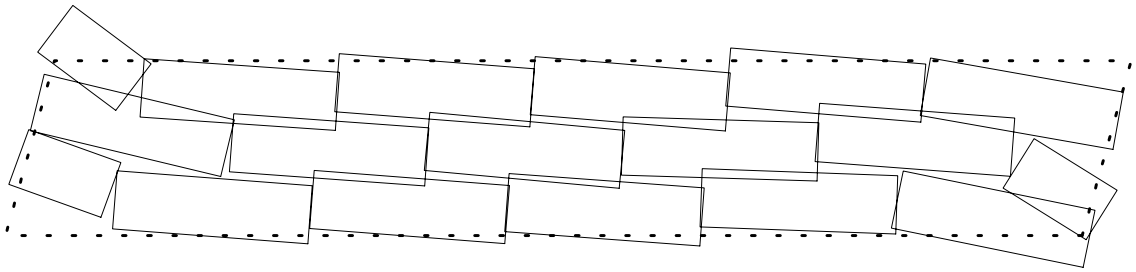

(a)

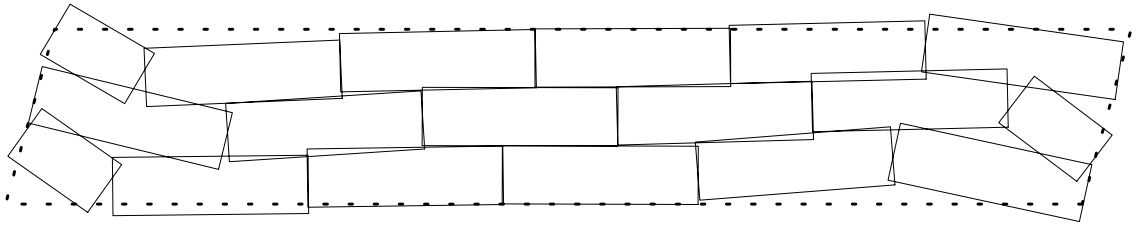

(b)

Figure 11. A sketch of final positions of blocks at $t = 2000$. Dotted line – the external boundary of the tectonic region. Displacements of blocks are exaggerated. Variants (c)–(d) (not shown) are similar to (b).

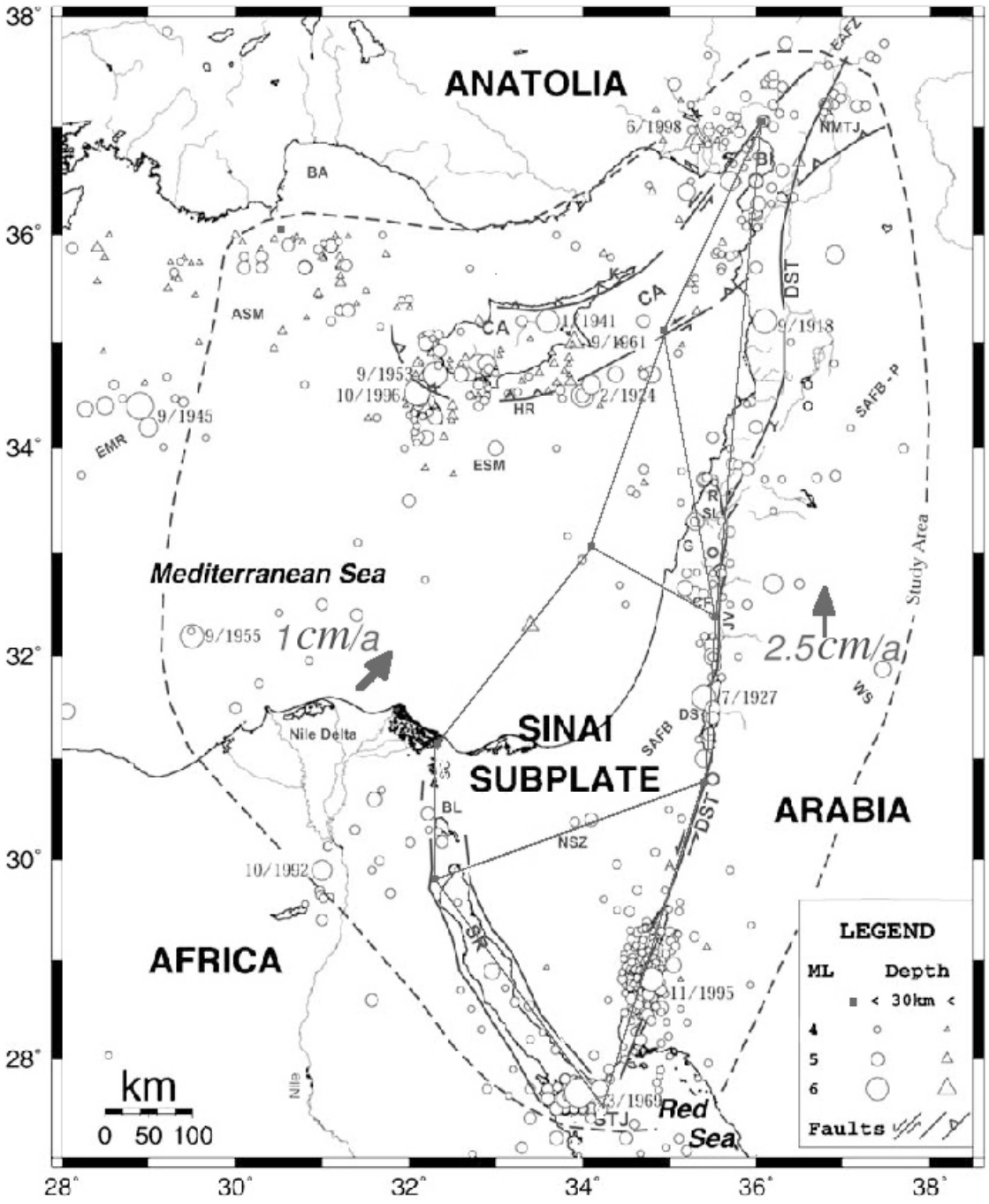

Figure 12. The Sinai Subplate.

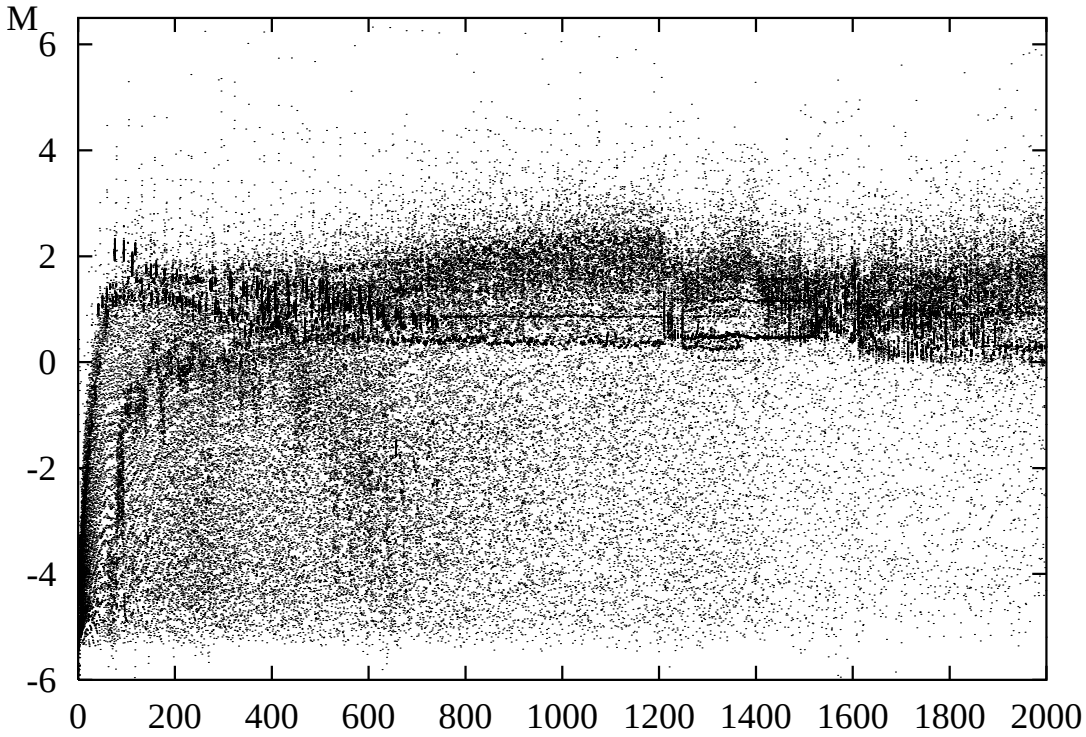

Figure 13. The magnitude versus time distribution for the synthetic catalog events (111296 events in total).

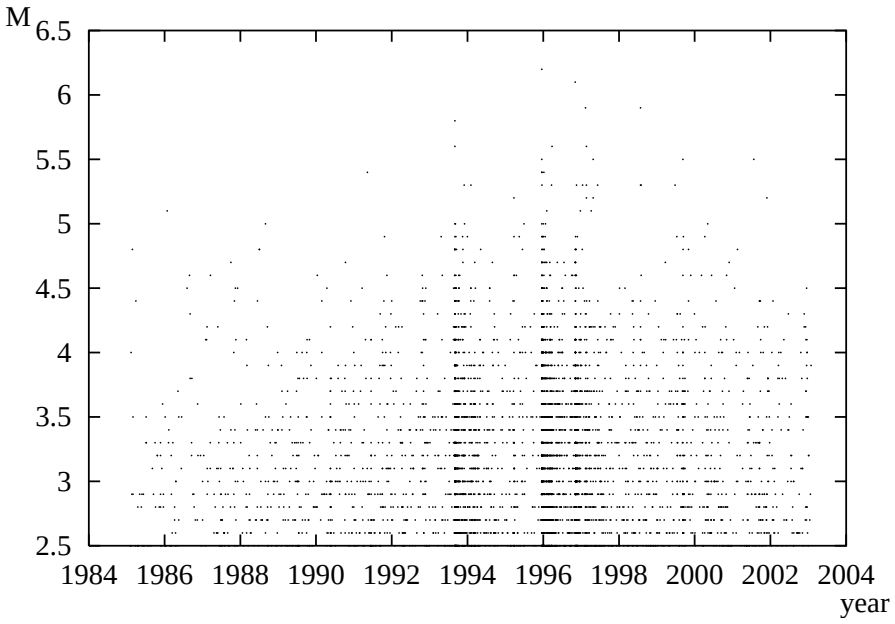

(a)

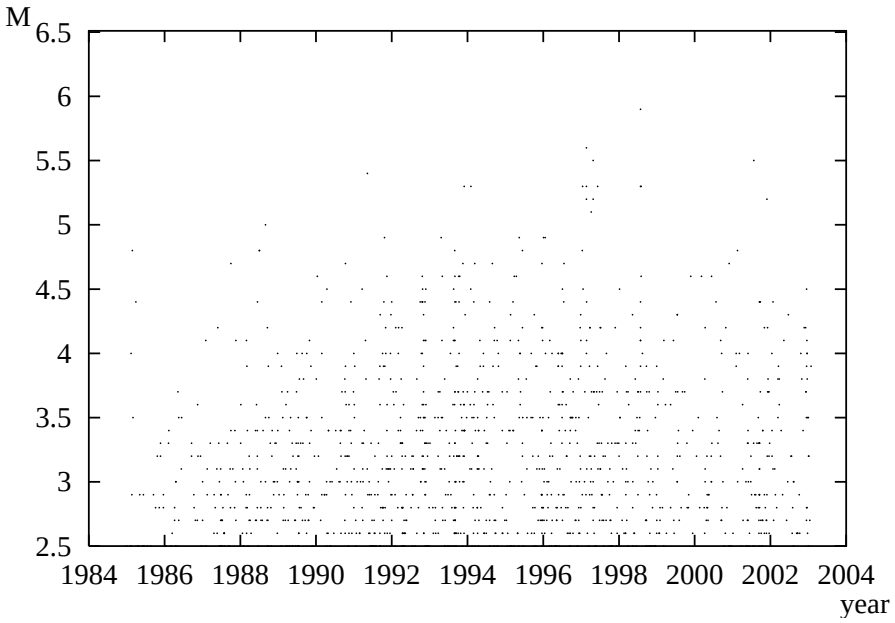

(b)

Figure 14. The magnitude versus time distribution for the real GII catalog events selected for the area, shown on Fig.12, for the period 1985-2002 (a) before filtering and (b) after filtering out the Cyprus Arc events and the Gulf of Aqaba events resampling (removing 29 out of 30 events). The total number of events of magnitude $ML > 2.5$ is 4694, after filtering 1256 events remain.

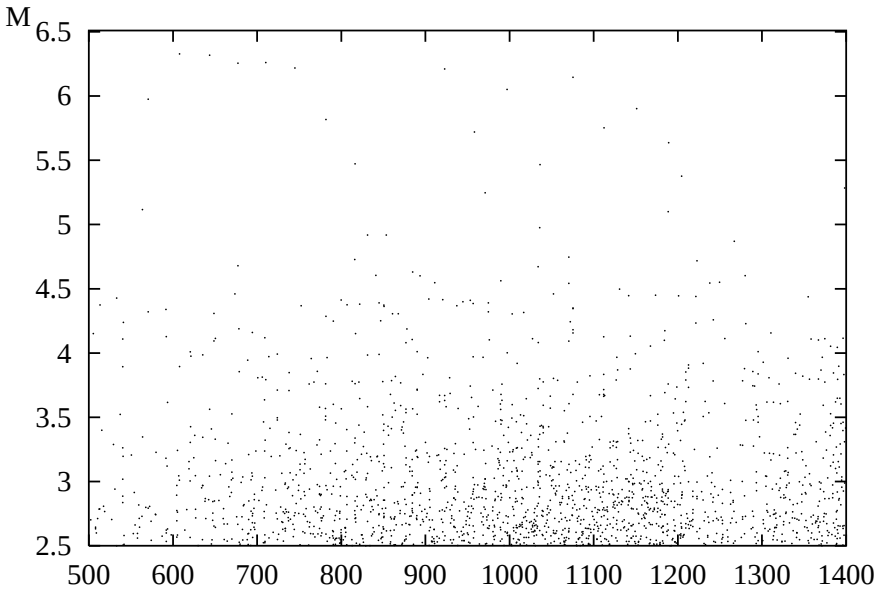

Figure 15. The magnitude versus time distribution for the synthetic catalog events for a span of 900 simulated time units.

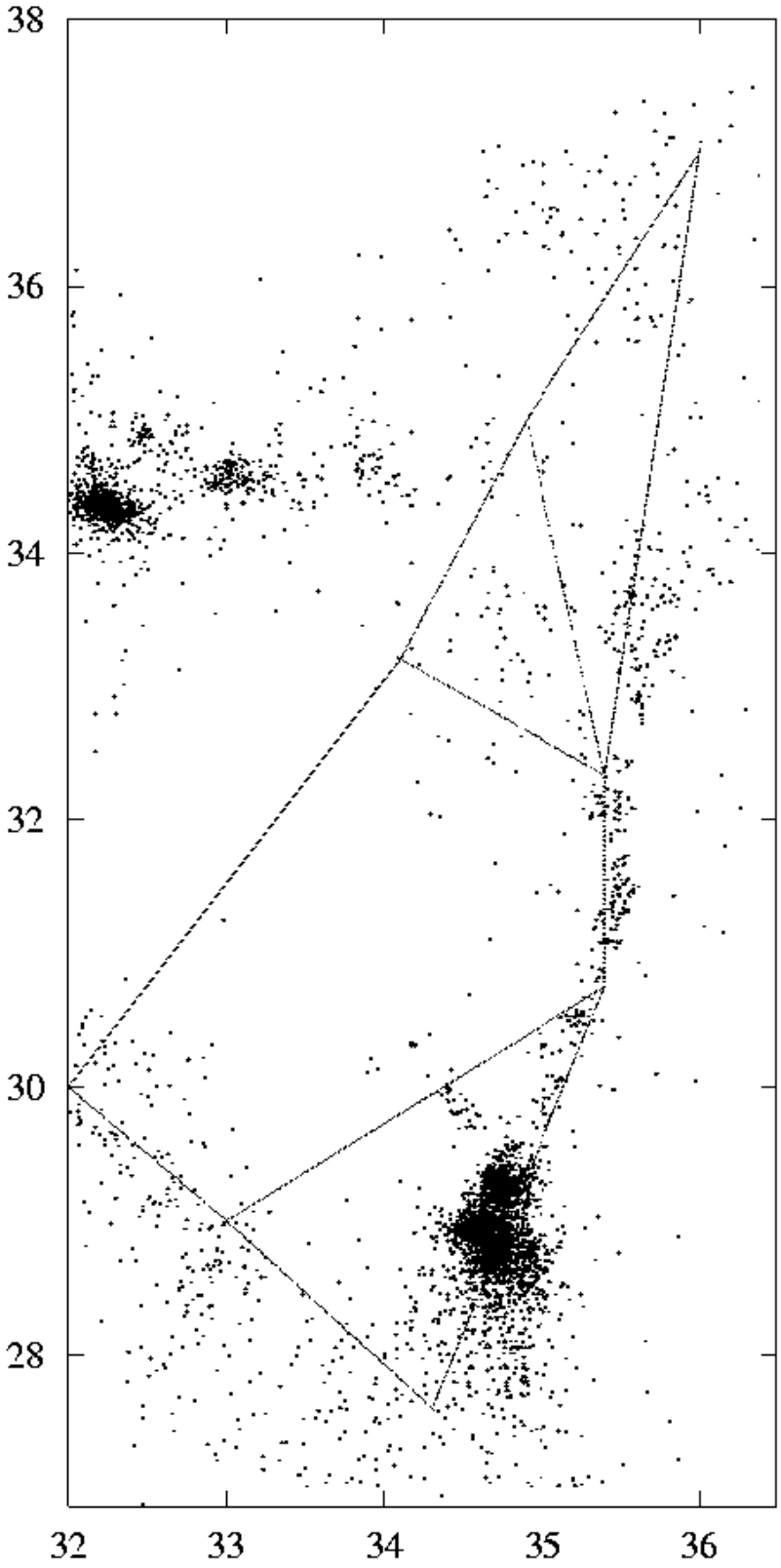

Figure 16. Lat-Long distribution of the GII catalog events with $ML > 2.5$ and the network of faults used for simulation.

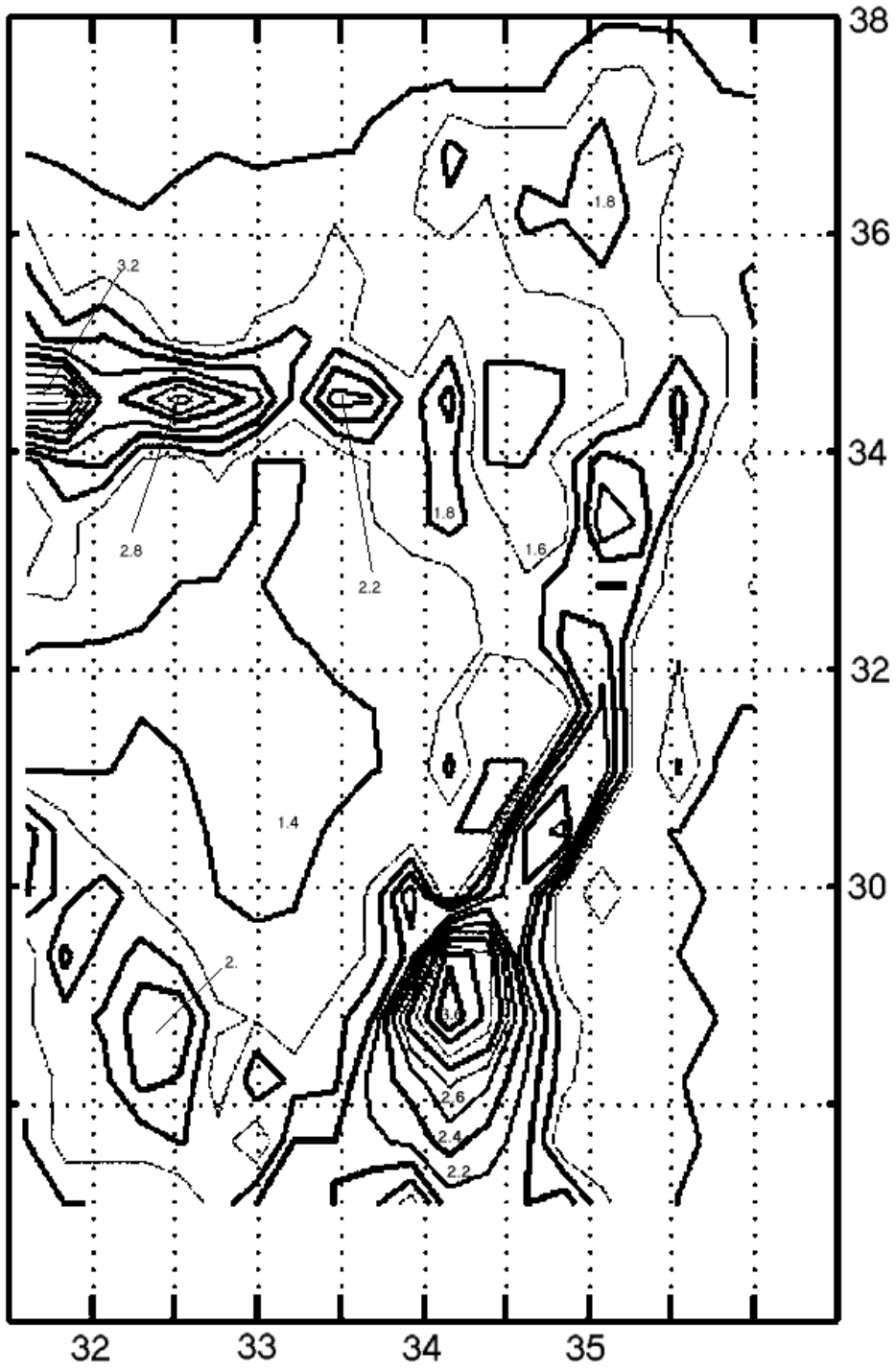

Figure 17. Spatial log density of the GII catalog for events with $ML > 2.5$.

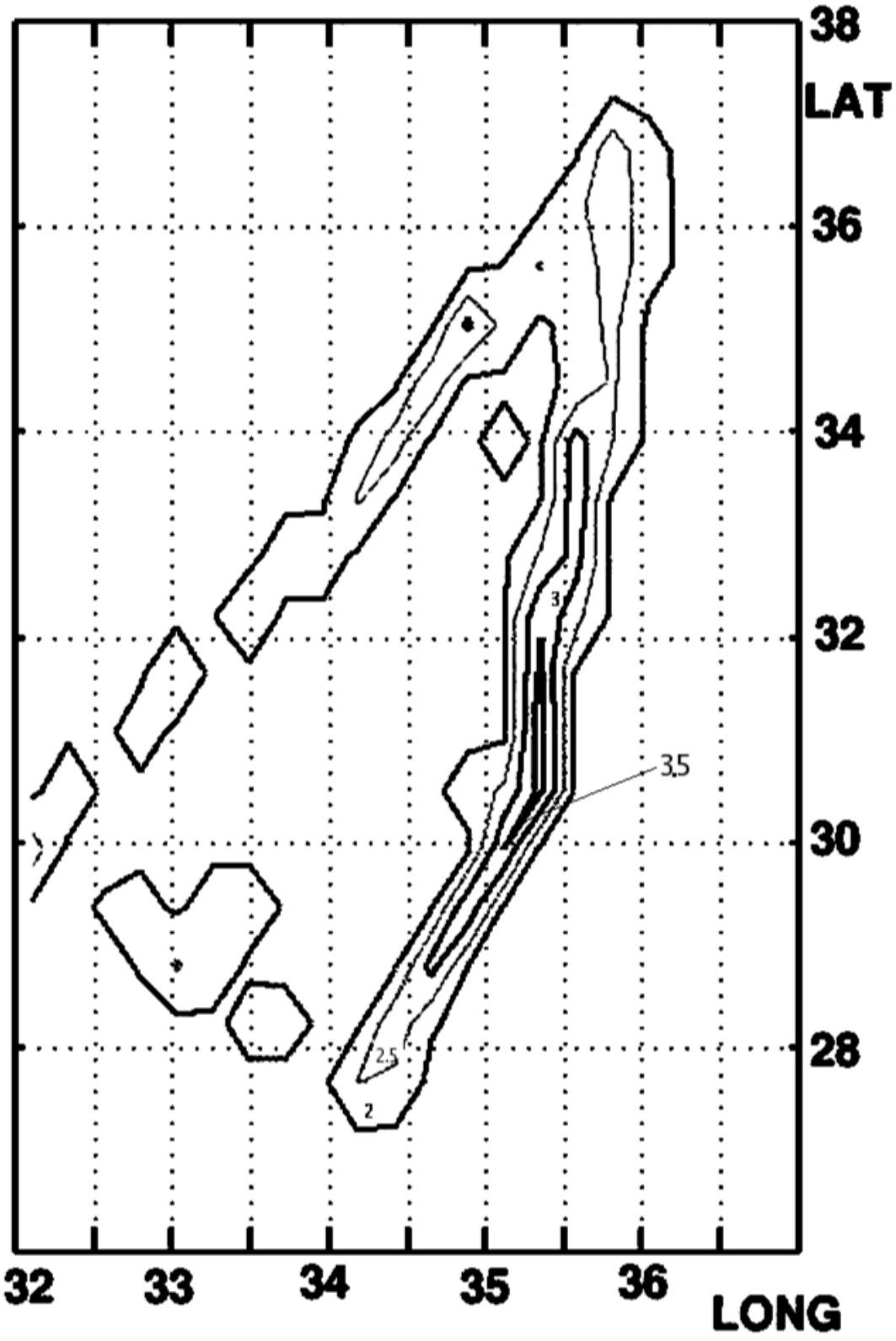

Figure 18. Equivalent spatial log density of the 2848 synthetic events.

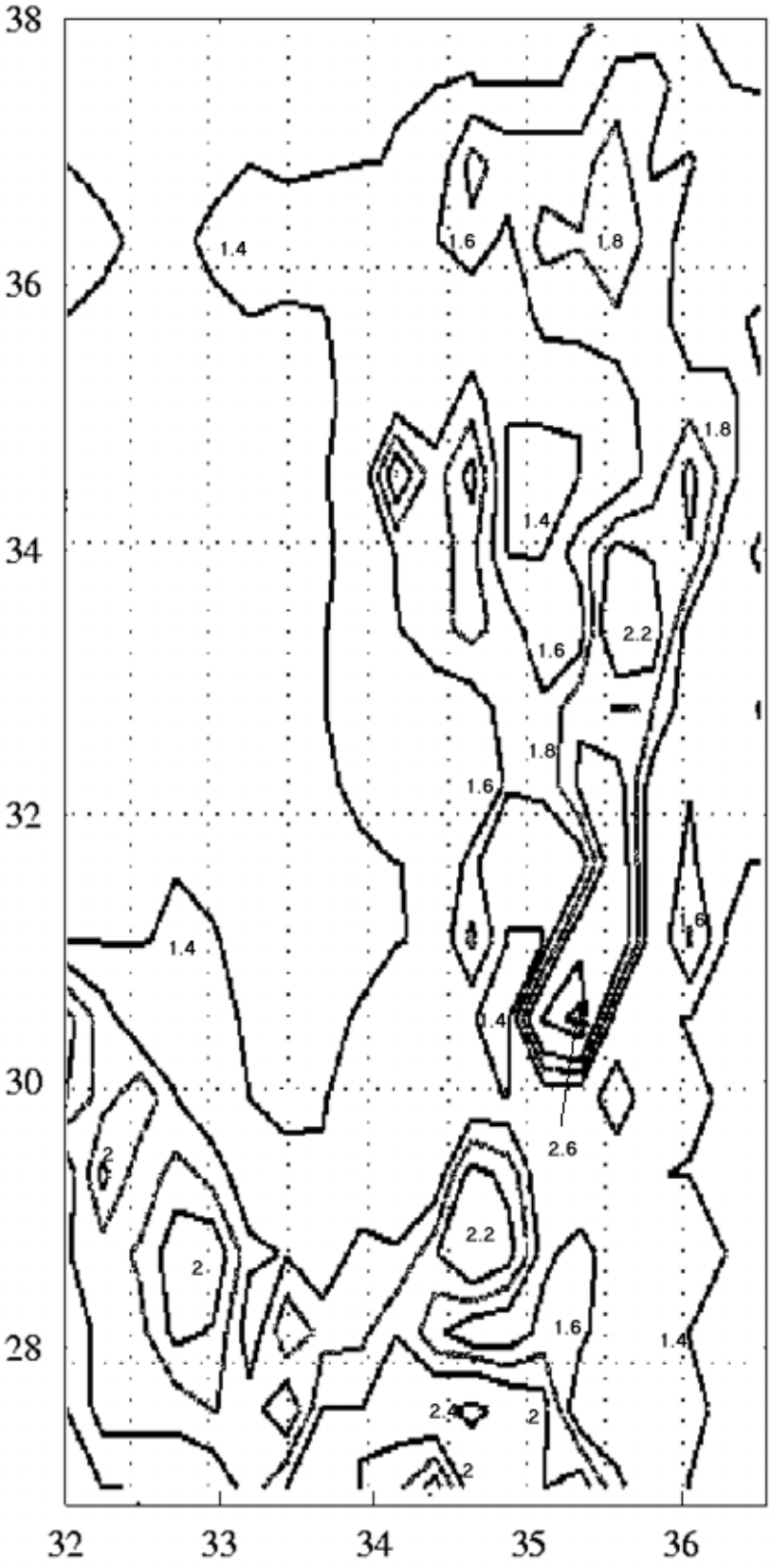

Figure 19. Spatial log density of the GII catalog after filtering out the Cyprian Arc events and 29/30 of the Gulf of Aqaba events.

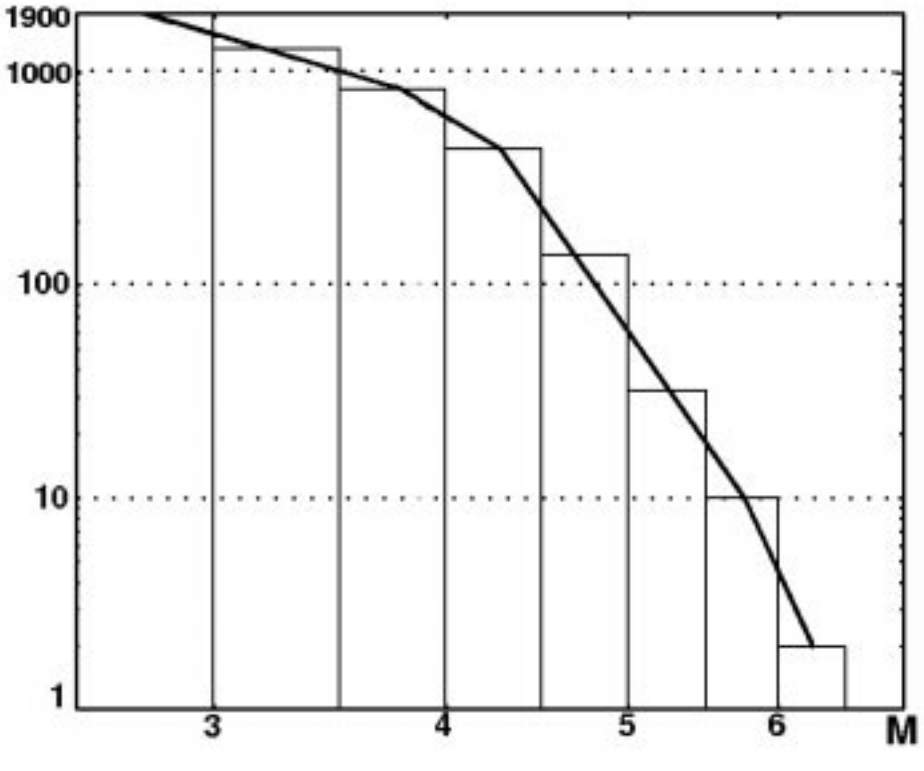

(a)

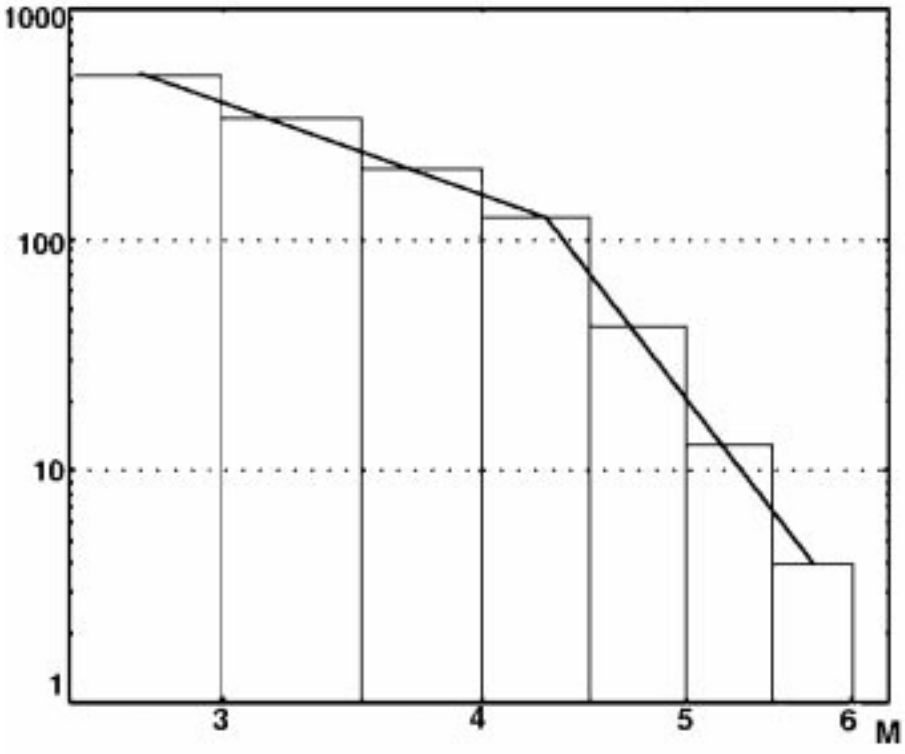

(b)

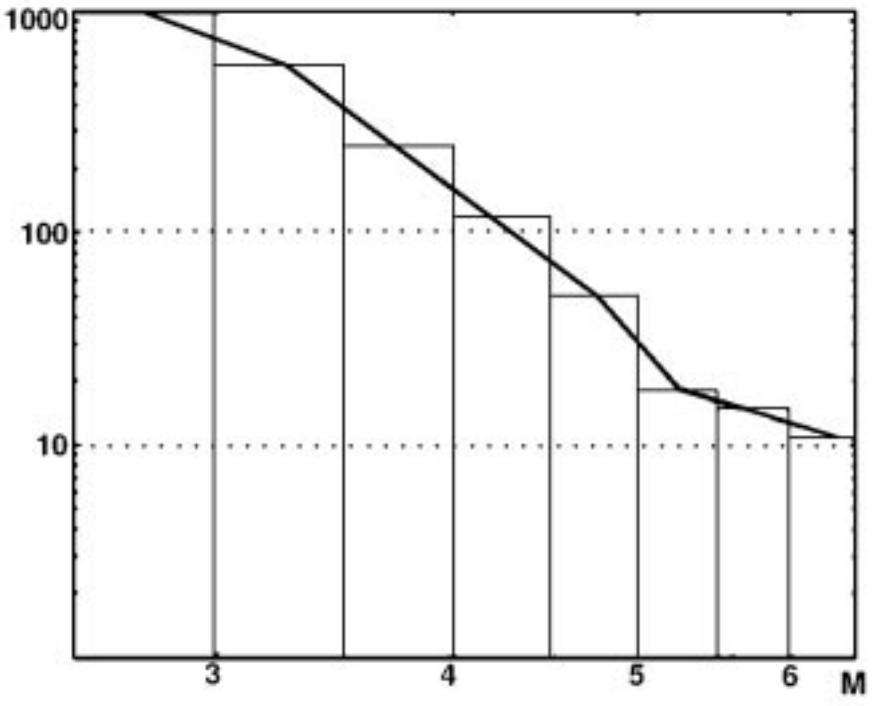

(c)

Figure 20. The number of events versus magnitude distribution for (a) the unfiltered GII catalog; (b) the filtered GII catalog and (c) the synthetic catalog.

References

[1] Akishin P.G., Altaisky M.V., Antoniou I., Budnik A.D., Ivanov V.V. (1998). Simulation of earthquakes with cellular automata. *Discrete dynamics in nature and society*, **2**, 267-279.

[2] Alekseevskaya M.A., Gabrielov A.M., Gvishiani A.D., Gel'fand I.M., Rantsman E.Ya. (1977). Formal morphostructural zoning of mountain territories. *J. Geophys.*, **43**, 227-233.

[3] Bak P., Tang C., Wiesenfeld K. (1987). Self-organized criticality: an explanation of $1/f$ noise. *Phys. Rev. Lett.*, **59**, 381-384.

[4] Bak P., Tang C., Wiesenfeld K. (1988). Self-organized criticality. *Phys. Rev. A*, **38**, 364.

[5] Bak P., Tang C. (1989). Earthquakes as a self-organized critical phenomenon. *J. Geophys. Res.*, **94**, 15635-15637.

[6] Barenblatt G.I., Entov V.M., Ryzhik V.M. (1972). *The theory of nonstationary filtration of fluids and gases*. Nedra, Moscow (in Russian).

[7] Barenblatt G.I., Entov V.M., Ryzhik V.M. (1990). *Theory of fluid flows through natural rocks*. Kluwer Acad. Publ., Dordrecht, Boston.

[8] Barenblatt G.I., Keilis-Borok V.I., Monin A.S. (1983). Filtration model of the earthquake sequences, *Doklady Akademii Nauk*, **269**, $N4$, 831-834 (in Russian).

[9] Basniev K.S., Kochina I.N., Maksimov V.M. (1993). *Underground hydrodynamics*. Nedra, Moscow (in Russian).

[10] Bear J. (1972). *Dynamics of fluid in porous media*. Elsevier, NY.

[11] Ben-Avraham Z., Ginzburg A., Makris J., Eppelbaum, L. (2002). Crustal structure of the Levant Basin, eastern Mediterranean. *Tectonophysics*, **346**, 23-43.

[12] Ben-Menahem A., Aboodi E. (1981). Micro- and macroseismicity of the Dead Sea Rift and of coast eastern Mediterranean. *Tectonophysics*, **80**, 233-199.

[13] Ben-Zion Y., Henvey T.L., Leary L.C., Lund S.P. (1990). Observations and implications of water well and creepmeter anomalies in the Mojave segment of the San-Andreas fault zone. *Bull. Seismol. Soc. Amer.*, **80** 6, 1661-1676.

[14] Ben-Zion Y., Rice J.R. (1993). Earthquake failure sequences along a cellular fault zones in a three-dimensional elastic solid containing asperity and nonasperity regions. *J. Geophys. Res.*, **98** (B8), 14109-14131.

[15] Ben-Zion Y., Rice J.R. (1995). Slip patterns and earthquake populations along different classes of faults in elastic solids. *J. Geophys. Res.*, **100**, 12959-12983.

[16] Ben-Zion Y., Rice J.R. (1997). Dynamic simulations of slip on a smooth fault in an elastic solid. *J. Geophys. Res.*, **102** (B8), 17771-17784.

[17] Ben-Zion Y., Sammis C., Henyey T. (1999). Perspectives on the field of physics of earthquakes. *Seismol. Res. Lett.*, **70**, 428-431.

[18] Brown S.R., Scholz C.H., Rundle J.B. (1991). A simplified spring-block model of earthquakes. *Geophys. Res. Lett.*, **18**, 215-218.

[19] Burridge R., Knopoff L. (1967). Model and theoretical seismicity. *Bull. Seismol. Soc. Amer.*, **57**, 341-371.

[20] Cao T., Aki K. (1985). Seismicity simulation with a mass-spring model and a displacement hardening-softening friction law. *Pure Appl. Geophys.*, **122**, 10-24.

[21] Cao T., Aki K. (1986). Seismicity simulation with a rate- and state-dependent law. *Pure Appl. Geophys.*, **124**, 487-514.

[22] Caputo M. (1992). *Rend. Accad. Naz. Lincei*, **9** $N3$, 5-10.

[23] Carlson J.M., Langer J.S. (1989a). Properties of earthquakes generated by fault dynamics. *Phys. Rev. Lett.*, **62**, 2632-2635.

[24] Carlson J.M., Langer J.S. (1989b). A mechanical model of an earthquake fault. *Phys. Rev. A*, **40**, 6470-6484.

[25] Carlson J.M., Langer J.S., Shaw B.E., Tang C. (1991). Intrinsic properties of a Burridge-Knopoff model of an earthquake fault. *Phys. Rev. A*, **44**, 884-897.

[26] Carlson J.M. (1991). A two-dimensional model of a fault. *Phys. Rev. A*, **44**, 6226-6232.

[27] Chen K., Bak P., Obukhov S.P. (1991). Self-organized criticality in a crack propagation model of earthquakes. *Phys. Rev. A*, **43**, 625-630.

[28] Christensen K., Olami Z. (1992). Variation of the Gutenberg-Richter b values and non-trivial temporal correlations in a spring-block model for earthquakes. *J. Geophys. Res.*, **97**, 8729-8735.

[29] Cochard A., Madariaga R. (1994). Dynamic faulting under rate-dependent friction. *Pure Appl. Geophys.*, **142** (3-4), 419-446.

[30] Cochard A., Madariaga R. (1996). Complexity of seismicity due to highly rate-dependent friction. *J. Geophys. Res.*, **101**, 25321-25336.

[31] Feder H.J.S., Feder J. (1991). Self-organized criticality in a stick-slip process. *Phys. Rev. Lett.*, **66** 20, 2669-2672.

[32] Fyfe W.S., Price N.J., Thompson A.B. (1978). *Fluids in the Earth's crust: their significance in metamorphic, tectonic and chemical transport processes.* Elsevier Sci. Publ. Co., North-Holland.

[33] Gabrielov A.M., Keilis-Borok V.I., Jackson D.D. (1996). Geometric incompatibility in a fault system. *Proc. Natl. Acad. Sci. USA*, **93**, 3838-3842.

[34] Gabrielov A.M., Keilis-Borok V.I., Levshina T.A., Shaposhnikov V.A. (1986). Block model of lithosphere dynamics. *Mathematical methods in seismology and geodynamics* (*Computational seismology*, **19**), Eds. V.I.Keilis-Borok, A.L.Levshin, 168-178. Nauka, Moscow (in Russian).

[35] Gabrielov A.M., Kosobokov V.G., Soloviev A.A. (1993). Interpretation of the block structure of a region by a block model of lithosphere dynamics. *Mathematical modeling of seismotectonic processes in lithosphere, aiming at the problem of earthquake prediction*, **1**, 11-19. IIEPT RAS, Moscow (in Russian).

[36] Gabrielov A.M., Levshina T.A., Rotwain I.M. (1989). Block model of lithosphere dynamics and earthquake prediction. *Theory and algorithms for interpretation of seismological data* (*Computational seismology*, **22**), Eds. V.I.Keilis-Borok, A.L.Levshin, 46-55. Nauka, Moscow (in Russian).

[37] Gabrielov A.M., Levshina T.A., Rotwain I.M. (1990). Block model of earthquake sequence. *Physics of the Earth and Planetary Interiors*, **61**, 18-28.

[38] Gabrielov A.M., Newman W.I. (1994). Seismicity modeling and earthquake prediction: a review. *Nonlinear dynamics and predictability of geophysical phenomena*. AGU, Washington, 7-14.

[39] Gabrielov A.M., Newman W.I., Knopoff L. (1994). Lattice model of failure: Sensitivity to the local dynamics. *Phys. Rev. E*, **50**, 188-197.

[40] Garianova T.V., Rotwain I.M. (1998). The properties of seismicity for the simplest type tectonic motion. The block model and reality. *Problems in geodynamics and seismology* (*Computational seismology*, **30**), Eds. V.I.Keilis-Borok, G.M.Molchan, 289-299. Geos, Moscow (in Russian).

[41] Gasilov V., Maksimov V., Kossobokov V., Prozorov A., Soloviev A. (1995). Numerical simulation of block structure dynamics. II. Examples. *Third Workshop on non-linear dynamics and earthquake prediction*, 6-17 November 1995. H4.SMR/879-3. ICTP, Trieste.

[42] Gasilov V.L., Prozorov A.G., Soloviev A.A. (1996). Local interaction of seismic events in synthetic catalog of a model of block structure dynamics. *Modern problems of seismicity and Earth dynamics* (*Computational seismology*, **28**), Eds. V.I.Keilis-Borok, G.M.Molchan, 110-130. Nauka, Moscow (in Russian).

[43] Gear V. (1971). Numerical initial value problems in ordinary differential equations. Prentice-Hall, Englewood Cliff.

[44] Ghertzik V.M. (1993). Foreshocks and aftershocks in a stratified Burridge-Knopoff model. *Mathematical modeling of seismotectonic processes in lithosphere, aiming at the problem of earthquake prediction*, **1**, 20-23. IIEPT RAS, Moscow (in Russian).

[45] Ghertzik V.M. (1994). Delocalization, foreshocks and aftershocks in a modified Burridge-Knopoff model. *Theoretical problems of geodynamics and seismology* (*Computational seismology*, **27**), Eds. V.I.Keilis-Borok, A.L.Levshin, 127-136. Nauka, Moscow (in Russian).

[46] Ghertzik V.M. (1998). Strange attractor and event clustering in the spring-block model with healing. *Problems in geodynamics and seismology* (*Computational seismology*, **30**), Eds. V.I.Keilis-Borok, G.M.Molchan, 264-274. Geos, Moscow (in Russian).

[47] Ginat H., Enzel Y., Avni Y. (1998). Translocated Pio-Pleistocene drainage systems along the Arava fault of the Dead Sea Transform. *Tectonophisics*, **284**, 151-160.

[48] Hertz A.V.M., Hopfield J.J. (1995). Earthquake cycles and neural reverberations: collective oscillations in systems with pulse-coupled threshold elements. *Phys. Rev. Lett.*, **75**, 1222-1225.

[49] Huang J., Narkounskaya G., Turcotte D.L. (1992). A cellular-automata, slider-block model for earthquakes. 2. Demonstration of self-organized criticality for a 2D system. *Geophys. J. Res. International*, **111**, 259-269.

[50] Ida Y. (1978). Propagation of slip along frictional surfaces. *Pure Appl. Geophys.*, **116**, 943-945.

[51] Ismail-Zadeh A.T., Keilis-Borok V.I., Soloviev A.A. (1999). Numerical modelling of earthquake flow in the southeastern Carpathians: effect of a sinking slab. *Physics of the Earth and Planetary Interiors*, **111**, 267-274.

[52] Ito K., Matsuzaki M. (1990). Earthquakes as a self-organized critical phenomena. *J. Geophys. Res.*, **95**, 6853-6860.

[53] Ito K. (1992). Towards a new view of earthquake phenomena. *Pure Appl. Geophys.*, **138**, 531-548.

[54] Joffe S., Garfunkel Z. (1987). Plate kinematics of the circum Red Sea – a reevaluation. *Tectonophysics*, **141**, 5-22.

[55] Johnson A.G., Kovach R.L., Nur A. (1974). Fluid-pressure variations and fault creep in central California. *Tectonophysics*, **23**, 257-266.

[56] Kasahara K. (1981). *Earthquake mechanics.* Cambridge Univ. Press.

[57] Keilis-Borok V.I. (1990a). Introduction: Non-linear systems in the problem of earthquake prediction. *Physics of the Earth and Planetary Interiors*, **61**, 1-7.

[58] Keilis-Borok V.I. (1990b). The lithosphere of the Earth as a non-linear system with implications for earthquake prediction. *Rev. Geophys.*, **28**, 19-34.

[59] Keilis-Borok V.I. (1994). Symptoms of instability in a system of earthquake-prone faults. *Physica D*, **77**, 193-199.

[60] Keilis-Borok V.I., Rotwain I.M., Soloviev A.A. (1997). Numerical modeling of block structure dynamics: dependence of a synthetic earthquake flow on the structure separateness and boundary movements. *J. Seismol.*, **1** 2, 151-160.

[61] Knopoff L. (1996). The organization of seismicity on fault networks. *Proc. Natl. Acad. Sci. USA*, **93**, 3830-3837.

[62] Kochina P.Ia. (1962). *Theory of ground water movement.* Princeton Univ. Press.

[63] Landau L.D., Lifshitz E.M. (1976). *Mechanics*. Pergamon Press, Oxford, NY.

[64] Langer J.S., Carlson J.M., Myers C.R., Shaw B.E. (1996). Slip complexity in dynamic models of earthquake faults. *Proc. Natl. Acad. Sci. USA*, **93**, 3825-3829.

[65] Lomnitz-Adler J., Knopoff L., Martinez-Mekler J. (1992). Avalanches and epidemic models of fracturing in earthquakes. *Phys. Rev. A*, **45**, 2211-2221.

[66] Lyakhovsky V., Ben-Zion Y., Agnon A. (2001). Earthquake cycle, fault zones, and seismicity patterns in a rheologically layered lithosphere. *J. Geophys. Res.*, **106** (B3), 4103-4120.

[67] Madariaga R., Cochard A. (1994). Seismic source dynamics, heterogenity and friction. *Ann. Geofis.*, **37**, 1349-1375.

[68] Madariaga R., Cochard A. (1996). Dynamic friction and the origin of the complexity of earthquake sources. *Proc. Natl. Acad. Sci. USA*, **93**, 3819-3824.

[69] Maksimov V.I., Soloviev A.A. (1996). Clustering of earthquakes in a block model of lithosphere dynamics. *Modern problems of seismicity and Earth dynamics* (*Computational seismology*, **28**), Eds. V.I.Keilis-Borok, G.M.Molchan, 148-152. Nauka, Moscow (in Russian).

[70] Miller S.A., Ben-Zion Y., Burg J.-P. (1999). A three-dimensional fluid-controlled earthquake model: Behavior and implications. *J. Geophys. Res.*, **104**, 10621-10638.

[71] Myers C.R., Langer J.S. (1993). Rupture propagation, dynamical front selection and the role of small length-scales in a model of an earthquake fault. *Phys. Rev. E*, **47**, 30-48.

[72] Nakanishi H. (1990). Cellular-automaton model of earthquakes with deterministic dynamics. *Phys. Rev. A*, **41**, 7086-7089.

[73] Nakanishi H. (1991). Statistical properties of the cellular-automaton model for earthquakes. *Phys. Rev. A*, **43**, 6613-6621.

[74] Narkounskaya G., Huang J., Turcotte D.L. (1992). Chaotic and self-organized critical behavior of a generalized slider-block model. *J. Stat. Phys.*, **67**, 1151-1183.

[75] Nielsen S., Knopoff L., Tarantola A. (1995). Model of earthquake recurrence: Role of elastic wave radiation, relaxation of friction, and inhomogeneity. *J. Geophys. Res.*, **100** (B7), 12423-12430.

[76] Nikolaevskii V.N. (1990). *Mechanics of porous and fractured media.* World Scientific, Singapore.

[77] Nikolaevskii V.N. (1996). *Geomechanics and fluidodynamics: with applications to reservoir engineering.* Kluwer Acad. Publ., Dordrecht, Boston.

[78] Nikolaevskii V.N., Basniev K.S., Gorbunov A.T., Zotov G.A. (1970). *Mechanics of saturated porous media.* Nedra, Moscow (in Russian).

[79] Nur. A. (1973). Role of pore fluids in faulting. In *Phil. Trans. R. Soc. Lond.* **A274**, Proceedings of the conference on tectonic problems of the San Andreas Fault. Eds. Kovach R.J., Nur A., 297-304.

[80] Nur A. (1978). Nonuniform friction as a physical basis for earthquake mechanics. *Pure Appl. Geophys.*, **116**, 964-989.

[81] Nur A., Booker J.R. (1972). Aftershocks caused by pore fluid flow? *Science*, **175 (4024)**, 885-887.

[82] Nur A., Ron H., Scotti O. (1989). Mechanics of distributed fault and block rotation. In *Paleomagnetic rotations and continental deformation*, Eds. Kissel C., Laj C., 209-228, Kluwer Academic Publishers.

[83] Li Y., Geissman J.W., Nur A., Ron H., Huang Q. (1990). Paleomagnetic evidence for counterclockwise block rotation in the North Nevada rift region. *Geology*, **18**, 79-82.

[84] Olami Z., Christensen K. (1992). Temporal correlations, universality and multifractality in a spring-block model of earthquakes. *Phys. Rev. A*, **46**, 1720-1723.

[85] Olami Z., Feder H.J.S., Christensen K. (1992). Self-organized criticality in a continuous, non-conservative cellular automaton modelling earthquakes. *Phys. Rev. Lett.*, **68** 8, 1244-1247.

[86] Osika D.G. (1981). *Fluid regime of seismic active regions*. Nauka, Moscow (in Russian).

[87] Otsuka M. (1972). A simulation of earthquake occurrence. *Physics of the Earth and Planetary Interiors*, **6**, 311-315.

[88] Panza G.F., Soloviev A.A., Vorobieva I.A. (1997). Numerical modelling of block-structure dynamics: application to the Vrancea region. *Pure Appl. Geophys.*, **149**, 313-336.

[89] Press W.H., Teukolsky S.A., Vetterling W.T. & Flannery B.P. (1992). *Numerical Recipes*, Cambridge Univ. Press.

[90] Rice J.R. (1992). Fault stress states, pore pressure distributions and the weakness of the San Andreas Fault. In *Fault mechanics and transport properties of rocks; A festschrift in honour of W.F.Brace*, Eds. B.Evans, T.-F.Wong, 475-503, Academic Press, NY.

[91] Rice J.R. (1993). Spatio-temporal complexity of a slip on a fault. *J. Geophys. Res.*, **98** (B6), 9885-9907.

[92] Rice J.R., Ben-Zion Y. (1996). Slip complexity in earthquake fault models. *Proc. Natl. Acad. Sci. USA*, **93**, 3811-3818.

[93] Rice J.R., Simons D.A. (1976). The stabilization of the spreading shear faults by coupled deformation-diffusion effects in fluid-infiltrated porous materials. *J. Geophys. Res.*, **81**, 5322-5334.

[94] Robinson R., Benites R. (1995). Synthetic seismicity models of multiple interacting faults. *J. Geophys. Res.*, **100**, 18229-18238.

[95] Roeloffs E.A. (1988). Hydrologic precursors to earthquakes: a review. *Pure Appl. Geophys.*, **126**, 177-209.

[96] Roeloffs E. (1996). Poroelastic techniques in the study of earthquake-related hydrologic phenomena. *Advances in Geophys.*, **37**, 135-195.

[97] Rotwain I.M., Soloviev A.A. (1998). Numerical modeling of block structure dynamics: temporal characteristics of a synthetic earthquake flow. *Problems in geodynamics and seismology* (*Computational seismology*, **30**), Eds. V.I.Keilis-Borok, G.M.Molchan, 275-288. Geos, Moscow (in Russian).

[98] Rozenberg V., Soloviev A.A. (1997). Considering 3D movements of blocks in the model of block structure dynamics. *Fourth Workshop on non-linear dynamics and earthquake prediction*, 6-24 October 1997. H4.SMR/1011-3. ICTP, Trieste.

[99] Rundle J.B., Brown S.R. (1991). Origin of the rate dependence in frictional sliding. *J. Stat. Phys.*, **65**, 403-412.

[100] Rundquist D.V., Soloviev A.A. (1999). Numerical modeling of block structure dynamics: an arc subduction zone. *Physics of the Earth and Planetary Interiors*, **111**, 241-252.

[101] Rybakov M., Goldshmidt V., Fleischer L., Rotstein Y. (1999). Crystalline basement in central Israel derived from gravity and magnetic data. *Isr. J. Earth Sci.*, **48**, 101-111.

[102] Rybakov M., Fleischer L., Reznicov M., Segev A. (2002). Study of the crystalline basement in Israel and adjacent areas (continuation). Geophysical Institute of Israel, Report No. 840/199/01.

[103] Sadovsky M.A., Bolkhovitinov L.G., Pisarenko V.F. (1982). On discreteness properties of rocks. *Izvestiya Akademii Nauk SSSR, Fizika Zemli* 12, 3-18 (in Russian).

[104] Sadovsky M.A., Golubeva T.V., Pisarenko V.F., Shnirman M.G. (1984). Characteristic rock dimensions and hierarchy properties of seismicity. *Izvestiya Akademii Nauk SSSR, Fizika Zemli* 2, 3-15 (in Russian).

[105] Sadovsky M.A., Bolkhovitinov L.G. (1990). *Seismic process in a block medium.* Nauka, Moscow (in Russian).

[106] Salamon A., Hofstetter A., Garfunkel Z., Ron H. (2003). Seismotectonics of the Sinai subplate – the eastern Mediterranean region. *Geoph. J. Int.* **155**, 149-173.

[107] Schmittbuhl J., Vilotte J.-P., Roux S. (1996). A dissipation-based analysis of an earthquake fault model. *J. Geophys. Res.*, **101** (B12), 27741-27764.

[108] Scholz C.H. (1990). *The mechanics of earthquakes and faulting.* Cambridge Univ. Press.

[109] Scholz C.H. (1991). Earthquakes and faulting: Self-organized critical phenomena with a characteristic dimension. In *Spontaneous Formation of Space-Time structures and Criticality*, Eds. T.Riste, D.Sherrington, 41-56, Kluwer.

[110] Segall P., Rice J.R. (1975). Dilatancy, compaction and slip instability of a fluid-infiltrated fault. *J. Geophys. Res.*, **100** (B11), 22155-22171.

[111] Shaw B.E. (1993). Generalized Omori law for aftershocks and foreshocks from simple dynamics. *Geophys. Res. Lett.*, **20**, 907-910.

[112] Sobolev P.O., Soloviev A.A., Rotwain I.M. (1996). Modeling of lithosphere dynamics and seismicity for a region of Middle East. *Modern problems of seismicity and Earth dynamics* (*Computational seismology*, **28**), Eds. V.I.Keilis-Borok, G.M.Molchan, 131-147. Nauka, Moscow (in Russian).

[113] Soloviev A.A., Rundquist D.V. (1998). Modeling of seismicity of an arc subduction zone. *Doklady Akademii Nauk*, **362** 2, 256-260 (in Russian).

[114] Sornette A., Sornette D. (1989). Self-organized criticality and earthquakes. *Europhys. Lett.*, **9**, 197-202.

[115] Turcotte D.L. (1997). Fractals and chaos in geology and geophysics. Cambridge Univ. Press.

[116] Vasconcelos G.L., Vieira M.D., Nagel S.R. (1992). Phase-transitions in a spring block model of earthquake. *Physica A*, **191**, 69-74.

[117] Yamashita T. (1997). Mechanical effect of fluid migration on the complexity of seismicity. *J. Geophys. Res.*, **102** (B8), 17797-17806.

[118] Zheligovsky V.A., Podvigina O.M. (2002). A model of tectonic blocks dynamics with an account of fluid migration along the fault system. *Physics of the Earth*, *N*12, 3-13. (English translation: Zheligovsky V.A., Podvigina O.M. A model for the dynamics of tectonic blocks incorporating fluid migration through a fault system. *Izvestiya, Physics of the Solid Earth* **38** *N*12, 2002, 995-1005.)